DEVELOPMENT OF A NOVEL COMPACT REFORMER FOR PEMFC

By

JING SU

A DISSERTATION PRESENTED TO THE GRADUATE SCHOOL
OF THE UNIVERSITY OF FLORIDA IN PARTIAL FULFILLMENT
OF THE REQUIREMENTS FOR THE DEGREE OF
DOCTOR OF PHILOSOPHY

UNIVERSITY OF FLORIDA

2009

To my parents and my brother.

ACKNOWLEDGMENTS

I would like to express my gratitude to my supervisor Prof. Chang-Won Park, for his enthusiastic support and guidance throughout this study. He was always passionate and caring when I met difficulties. He was willing to share his experience and spent plenty of time in giving me instructions. I wish to thank my cochair Dr. Helena E. Hagelin-Weaver, for her abundantly helpful and invaluable assistance and suggestion. I also wish to thank Dr. Jason E. Butler and Prof. Renwei Mei for their valuable recommendation as dissertation committee members. Also, I would like to express my sincere thank to Mr. Samuel D. Jones for his assistance in gas chromatographic measurements. Special thank to Dr. Jong Kwan Lee for his assistance in preparing the experimental setup.

This study was partially supported by NASA Lewis/Glenn Research Center, Grant NAG 3-2930, through the College of Engineering at the University of Florida.

TABLE OF CONTENTS

page

LIST OF TABLES

LIST OF FIGURES

Abstract of Dissertation Presented to the Graduate School
of the University of Florida in Partial Fulfillment of the
Requirements for the Degree of Doctor of Philosophy

DEVELOPMENT OF A NOVEL COMPACT REFORMER FOR PEMFC

By

Jing Su

May, 2009

Chair: Chang-Won Park
Cochair: Helena Hagelin-Weaver
Major: Chemical Engineering

A compact reformer to produce hydrogen for portable fuel cell applications is presented in this thesis. This reformer is a conventional single-path tubular reactor type that is packed with granular catalyst particles. The catalyst is used to induce catalytic partial oxidation reaction (CPOX) and steam reforming reaction (SR) in series using a mixture of methanol, water and oxygen as the feed. One of the important features of the reformer is the interlaced flow path for efficient heat transfer between the reactor sections where the endothermic SR reaction and the exothermic CPOX reaction may be taking place, respectively. Flow simulation has been conducted to determine various design features including the dimension of the reformer that can be used for a PEMFC with the energy production capacity of 10 Watt at 50% efficiency. Subsequently, a prototype reformer has been built to confirm the simulation results and to assess the efficacies of new design features.

Experiment with a commercial catalyst ($CuO/ZnO/Al_2O_3$) showed a methanol conversion of about 85% at the feed rate enough to generate energy production capacity of 10 Watt at 50% efficiency with an operating temperature of 250°C or below, and a hydrogen concentration of approximately 72-73% in the product gas when SR is the only hydrogen generation reaction.

When oxygen is fed to the reformer as an additional reactant, CPOX reaction also takes place and the hydrogen concentration decreases slightly as a result. The current study showed a hydrogen concentration of approximately 67%-72% at 250ºC at various oxygen feed rates. These hydrogen concentrations in the product gas are in reasonable agreement with theoretical predictions and indicate that the CPOX reaction does indeed take place before the SR reaction. The experiments indicated that only 5 of the maximum 19 reformer channels filled with catalyst are not sufficient to complete both the CPOX and SR reactions under the conditions used in this study.

The experimental results support that the prototype reformer is capable of meeting the preset requirements to produce enough hydrogen for 10W PEMFC application. The results also suggest that proper insulation of the reformer is essential for self-sustainability.

CHAPTER 1
FUEL CELLS

A fuel cell is a device that can convert chemical energy directly into electrical energy. The first fuel cell may be dated back to 1839 when Sir William Grove, a British jurist and physicist, invented a system which converted chemical energy to electrical energy by reacting hydrogen and oxygen on platinum electrodes in a sulfuric acid solution [1-3]. At that time, the research on fuel cell was not as popular because the primary energy sources were abundant and readily available at a low cost. In the late 20th century, fuel cell emerged as an important technological area because of its capability to convert chemical energy directly into electrical energy with a higher efficiency than the conventional thermomechanical-electric devices [1]. The overall efficiency of a fuel cell for energy production is about two times higher than those of conventional combustion engines. Furthermore, fuel cells are environment-friendly as they use pure hydrogen as fuel and generate only water as a byproduct without producing any greenhouse gases. Renewable energy sources including wind, water and solar energy will continue to be developed quite extensively in the next few decades. However, these renewable energy resources may not fulfill the entire demand, and fuel cells may work as a complimentary energy source to those [3-7].

1.1 Types of Fuel Cell

Fuel cells may be classified into six different types. They are (1) Alkaline Fuel Cell (AFC), (2) Phosphoric Acid Fuel Cell (PAFC), (3) Molten Carbonate Fuel Cell (MCFC), (4) Solid Oxide Fuel Cell (SOFC), (5) Proton Exchange Membrane Fuel Cell (PEMFC) and (6) Direct Methanol Fuel Cell (DMFC). DMFC is in fact very similar to PEMFC thus it may belong to the same category as PEMFC [3-7]. This classification is based on the electrolytes used for each type of fuel cells. Some important features of each type of fuel cells are discussed below:

1.1.1 Alkaline Fuel Cell (AFC)

The alkaline fuel cell (AFC) is one of the most well developed fuel cell types, which was used for the Apollo mission in 1960s [6,8]. In an AFC system, hydrogen and oxygen supply not only electric power but also heat and water. Alkaline fuel cell, for which Potassium hydroxide (usually 30-45 wt. % in concentration) is used as the electrolyte, operates at a low temperature below 100°C. AFC has the highest electrical efficiency among all fuel cell types. However, it is very sensitive to impurities such as carbon dioxide that can react with KOH and produce carbonates. The carbonates are destructive to the electrolyte and the performance of the fuel cell decreases sharply as a result. Thus, it is necessary to use pure hydrogen and oxygen as reactants or to use an extra unit, such as an iron sponge system, to remove carbon dioxide from the system. Many different catalysts may meet the requirement of the AFC electrode. Thus, inexpensive catalysts can be used lowering the manufacturing cost of AFC compared to other types that have limited options such as PEMFC [9-11].

1.1.2 Phosphoric Acid Fuel Cell (PAFC)

PAFC may be the most broadly commercialized fuel cell technology. PAFC-based power plants have been constructed in many places around the world with outputs ranging from 50-200 kW for general use to 5-20 MW for large plants that can supply electricity, heat, and hot water to various buildings in town including hospitals [6]. Phosphoric acid, that is the electrolyte for PAFCs, begins to solidify at about 40°C. This makes the startup of PAFC to be difficult thereby restricting the PAFCs to operate continuously [8].

The electrochemical reactions of PAFC take place on highly dispersed electro-catalyst particles which is supported on carbon black. Platinum or its alloys are used as the catalyst for both electrodes; the anode and the cathode. The advantages of PAFCs include thermal stability, chemical stability and low volatility of phosphoric acid at the operating temperature of

150~200°C. PAFC is also considered as a low-temperature fuel cell as AFC, PEMFC and DMFC due to its low operating temperature [10-12].

1.1.3 Molten Carbonate Fuel Cell (MCFC)

As its name indicates, MCFC uses a molten carbonate as the electrolyte which is stabilized by an alumina-based matrix [6]. The typical operating temperature of MCFC is 600~700°C, which is much higher than those of AFC or PEMFC [8, 10]. This high temperature is required in order to achieve sufficient conductivity of the carbonate electrolyte. The high operation temperature also makes it possible to utilize the waste heat properly. Due to the high operating temperature, non-precious metals and oxides such as Ni and NiO can be used as the catalysts for both electrodes thereby making it cost-efficient [13-15].

Unlike most other fuel cells, hydrocarbon fuels can be used as the fuel for MCFCs as the hydrocarbon fuel can be converted to hydrogen within the fuel cell itself by an internal reforming process. Another advantage of MCFCs is that they are quite resistant to impurities such as carbon monoxide or carbon dioxide achieving the electrical efficiency of 50% to 70% with a combined cycle system [16, 17]. The primary disadvantage of MCFC is its poorer durability. The materials of construction for MCFCs should meet the requirements imposed by the high operating temperature. In addition, they should resistant to the corrosion by the liquid electrolyte. Otherwise, leakage of the electrolyte can be a major problem [18, 19].

1.1.4 Solid Oxide Fuel Cell (SOFC)

The solid oxide electrolytes for SOFCs, that is usually Y_2O_3-stablilized ZrO_2, are more stable than those of MCFCs [3, 6]. Furthermore, SOFCs are more durable than MCFCs because the corrosion issue caused by solid oxide electrolytes is less problematic than that by the liquid electrolytes for MCFCs. The electrodes of SOFCs are typically made of Ni-ZrO_2 ceramal and Sr-doped $LaMnO_3$ [3, 6]. As the operating temperature of SOFC is high, expensive catalysts are not

necessary thereby making it economical than other types such as PEMFC that require expensive precious metal catalysts [20, 21].

Due to the high operation temperature of SOFC, that is in the range of 700~1000°C, similar requirements are imposed on the materials of construction as those for MCFC. Furthermore, internal reforming process is also possible with SOFC thereby making it possible to use hydrocarbon fuels without a separate reformer unit to convert hydrocarbon to hydrogen [22, 23].

1.1.5 Proton Exchange Membrane Fuel Cell (PEMFC)

PEMFC is named after the electrolyte which is a proton exchange membrane. The same acronym also refers to polymer electrolyte membrane fuel cell [6]. PEMFCs are known to have a high power density at a very low operating temperature. These advantages make PEMFC more suitable for portable applications than any other fuel cells. The most important milestone in the development of PEMFC may be the invention of the membrane called Nafion by DuPont. Main component of the Nafion membrane is poly-tetrafluoroethylene (PTFE), and sulfonation of the material imparts high acidity to the membrane and also provides high conductivity [10, 11]. The electrodes for PEMFCs are generally porous for efficient diffusion of gaseous components and for better contact of hydrogen and oxygen with the noble metal catalyst that is usually platinum [24-26].

As the working temperature is as low as 60~120°C, PEMFCs can achieve a much faster startup than MCFCs or SOFCs. While pure hydrogen is the suitable fuel for PEMFCs, a special PEMFC can use methanol directly as the fuel without a separate fuel processor. This special type of PEMFC is known as Direct Methanol Fuel Cell (DMFC) [27-29]. DMFC has a similar operating temperature as PEMFC although it operates at a slightly higher temperature to improve power density. DMFCs use methanol solution in water (generally 1~2M) as the fuel [3]. The methanol reacts with water at anode to release protons, electrons and carbon dioxide whereas

hydrogen is oxidized at anode generating protons and electrons in PEMFC. DMFC has a lower efficiency because of permeation of the methanol through the membrane, which is called "methanol crossover" [30]. This methanol crossover is the most serious deficiency of DMFC. Methanol can lead to a mixed potential through the interference of methanol oxidation reaction with the oxygen reduction reaction at cathode. While many factors are related with the methanol crossover, membrane itself is the main focus of research to resolve the issue. For DMFCs, a thicker membrane is usually better to decrease the methanol crossover. As the methanol is consumed at anode, a high performance anode which can oxidize as much methanol in feed will also decrease crossover. Another approach is to develop a methanol-tolerant catalyst for cathode [3, 30].

AFC, PAFC and MCFC have been well developed already, whereas further development efforts for SOFC and PEMFC/DMFC are still ongoing. A brief comparison between various types of fuel cells is given in Table 1-1.

Table 1-1 Fuel cell types and selected features [8]

Type	Operating temperature (°C)	Fuel	Electrolyte	Mobile ion
PEMFC (Polymer Electrolyte Membrane Fuel Cell)	70-110	H_2, CH_3OH	Sulfonated polymers (Nafion^{TM})	$(H_2O)_nH^+$
AFC (Alkali Fuel Cell)	100-250	H_2	Aqueous KOH	OH^-
PAFC (Phosphoric Acid Fuel Cell)	150-250	H_2	H_3PO_4	H^+
MCFC (Molten Carbonate Fuel Cell)	500-700	Hydrocarbons, CO	$(Na, K)_2CO_3$	CO_3^{2-}
SOFC (Solid Oxide Fuel Cell)	700-1000	Hydrocarbons, CO	$(Zr, Y)O_{2-\delta}$	O^{2-}

1.2 Fundamentals of PEMFC and the Use of a Hydrocarbon Fuel

As indicated schematically in Figure 1-1, PEMFC which consists of three major parts; anode, cathode and electrolyte. At the anode, hydrogen is oxidized into protons releasing electrons:

$$H_2 \rightarrow 2H^+ + 2e^- \tag{1-1}$$

The electrons flow from the anode to the cathode through an external circuit (or a conductor); hence generating electrical current to drive an external load. The protons migrate toward the cathode through the proton exchange membrane. Oxygen is reduced at the cathode by combining with the electrons from the anode, and then forms water by reacting with the protons from the anode through the proton exchange membrane:

$$1/2O_2 + 2H^+ + 2e^- \rightarrow H_2O \tag{1-2}$$

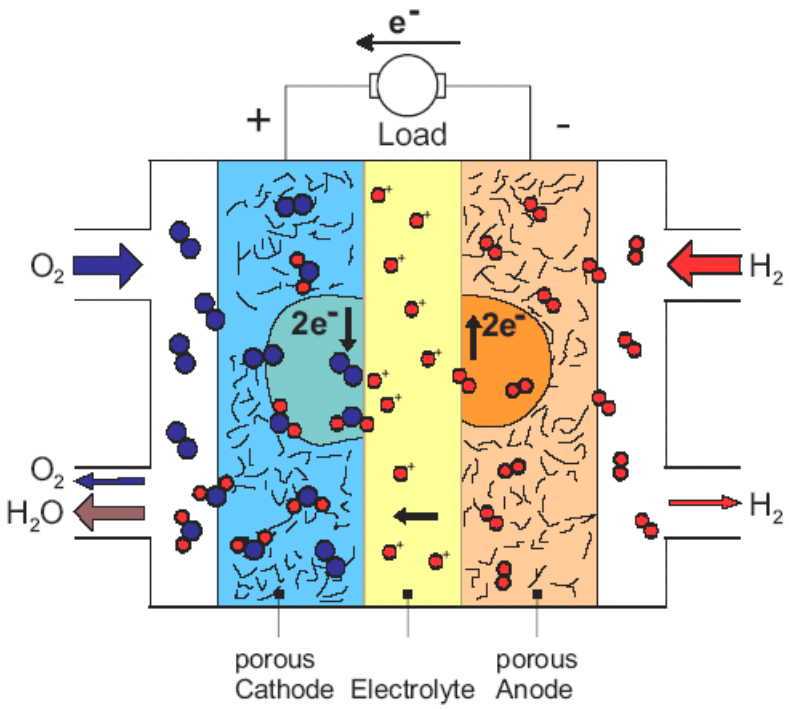

Figure 1-1 Schematic drawing of a hydrogen/oxygen fuel cell and its reactions based on the proton exchange membrane fuel cell (PEMFC) [3]

PEMFC offers much higher power density than other types of fuel cells. In addition, the intrinsic properties of the materials used for PEMFC make them operate at a low temperature between 60~120°C. This low operating temperature allows quick start-up and rapid load-response which are main advantages of PEMFC. Because of its low temperature operability, PEMFC is favored as a portable power source for the applications as in aviation, automobile, and consumer electronics (e.g. laptop, cell phones, etc…). In fact, only PEMFCs can meet the requirements for such portable applications which are compact size and lightweight besides low temperature operability.

The best fuel for PEMFC is pure hydrogen as for all other type of fuel cells. However, the storage of hydrogen as well as the portability of the hydrogen storage systems are rather problematic for small-size mobile applications. Thus, hydrocarbons, especially methanol or methane, are recognized as more practical choices as a fuel for PEMFCs [31, 32]. Use of methanol or other hydrocarbon fuels, however, requires a reformer unit by which hydrogen is produced. It is an additional unit that not only increases the system size but also creates other technical difficulties such as CO-poisoning of catalyst. Recent advances in various areas including catalyst technology have resolved many of the difficulties although there still exist some obstacles that require research efforts at a fundamental level. Between methanol and methane, methanol may be more favorable because it is in liquid phase at standard condition [33]. It is also much more difficult to reform methane. Steam reforming of methane requires more energy and significantly higher temperatures compared to methanol reforming [34-37]. Therefore, the current research has focused on reforming methanol.

The well-known reaction to produce hydrogen from methanol is the steam reforming reaction: [38-41]

$$CH_3OH + H_2O \rightarrow CO_2 + 3H_2 \quad (\Delta H_0 = 130.9 \text{ kJ/mol}) \tag{1-3}$$

The steam reforming of methanol is commonly carried out over commercially available low-temperature shift copper-based catalysts [42, 43]. The steam reforming reaction can be followed by a reverse shift reaction which establishes the thermodynamic equilibrium:

$$CO_2 + H_2 \leftrightarrow CO + H_2O \tag{1-4}$$

Another side reaction that is known to occur is the decomposition of methanol [6, 44]:

$$CH_3OH \rightarrow CO + 2H_2 \tag{1-5}$$

This reaction is known to occur when there exist excessive amounts of methanol in the system, i.e. at low H_2O and O_2 concentrations [45]. CO generated by the reaction (1-4) or (1-5) should be removed as it acts as a poison for the electrode catalyst in the fuel cell.

The steam reforming reaction occurs at about 200~300°C and it is an endothermic reaction requiring external heat supply. Although the heat can be supplied by an external source through the partial use of the electric power generated by the fuel cell, the catalytic partial oxidation (CPOX) of methanol that is highly exothermic (autothermal reforming) can be combined with the steam reforming reaction: [46-52]

$$CH_3OH + 1/2\ O_2 \rightarrow CO_2 + 2H_2 \quad (\Delta H_0 = -154.9 \text{ kJ/mol}) \tag{1-6}$$

Among the four reactions described above, only three reactions are linearly independent. Thus, in analyzing the flow rates and output gas compositions using material balances, only three reaction stoichiometries may be used (i.e., reactions 1-3 and 1-6 plus reaction 1-4 or 1-5).

The combustion reaction or total oxidation of methanol is also a side reaction that may take place in the presence of excess oxygen:

$$2CH_3OH + 3O_2 \rightarrow 2CO_2 + 4H_2O \tag{1-7}$$

This reaction consumes methanol and oxygen without producing hydrogen. Thus, it should be avoided, if at all possible.

The formaldehyde, HCHO may also be formed by the following side reactions: [53, 54, 55]

$$CH_3OH + 1/2O_2 \rightarrow HCHO + H_2O \quad (1\text{-}8)$$

$$CH_3OH \rightarrow HCHO + H_2 \quad (1\text{-}9)$$

This first formaldehyde-forming reaction consumes methanol and oxygen without producing any hydrogen and should also be avoided. While the dehydrogenation of methanol does produce hydrogen, the formaldehyde must be reformed in a second step to obtain the maximum hydrogen production rate.

Because the steam reforming reaction is reversible, a higher ratio of water to methanol may be preferable in order to obtain a high conversion of methanol at a low temperature. The study of Choi et al. [56], in fact, showed that the methanol conversion increased with the water content at a fixed reaction temperature as indicated in Figure 1-2. At a certain Gas Hourly Space Velocity (GHSV = volume of gas over volume of catalyst in one hour), a near-complete conversion of methanol is achieved at a lower temperature when the water content is higher [56]. Furthermore, the methanol decomposition and the reverse water-gas-shift reactions are suppressed in the presence of excess water [57, 58]. Thus, a higher water content in the feed is desired to decrease the operation temperature of a reformer while maintaining a high conversion of methanol, and suppress the CO forming reactions. However, by adding more water than the stoichiometric need, the reactor will require more energy to evaporate the excessive water. In actual reactor design, the improvement of conversion and selectivity must be sufficient to offset the additional energy load for evaporating the additional water for this to be economical.

The reverse shift reaction (Reaction 1-4) and the methanol decomposition reaction (Reaction 1-5) produce carbon monoxide that acts as a poison to the catalyst in the anode for the hydrogen oxidation reaction. The gas clean-up may be achieved by selective oxidation using a membrane where CO is removed from H_2 by selective oxidation using a catalytically active membrane [59], or methanation [60]. Selective oxidation of carbon monoxide can be achieved by alumina-supported Ru/Rh catalyst which provides near complete conversion of CO at a temperature as low as 100°C [61]. Therefore, a reformer may have to include a gas clean-up unit at the end of the reaction path where the steam reforming and/or the partial oxidation reactions are taking place.

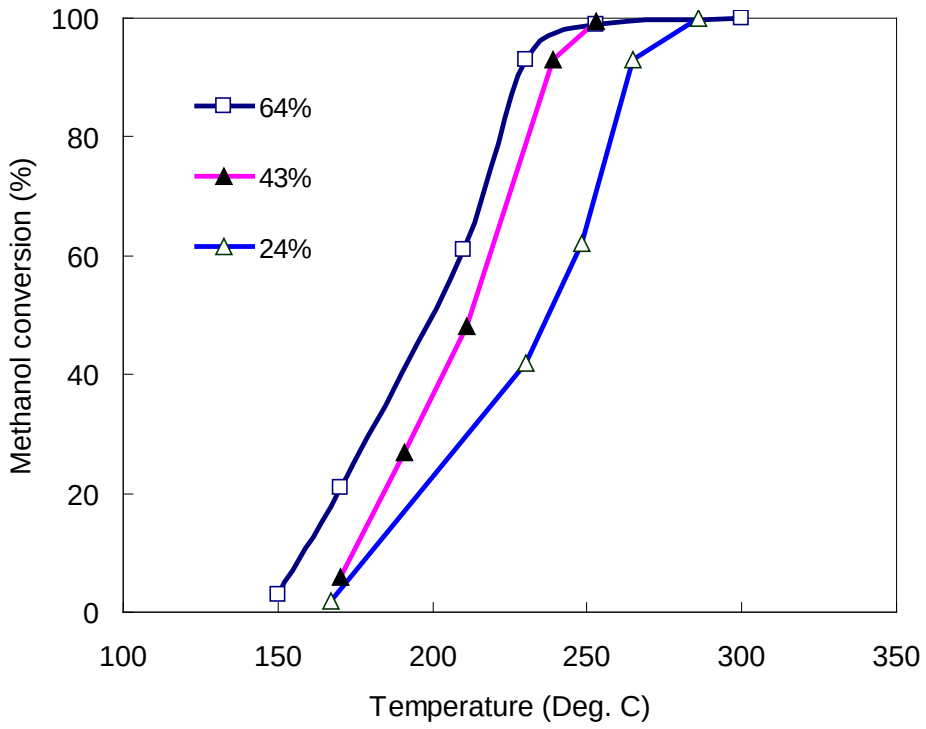

Figure 1-2 Methanol conversion in methanol steam reaction as a function of reaction temperature (water content in feed=24, 43, 64 mol%, catalyst loading =1.0 g, GHSV = 1100 h^{-1}). Conversion data are from Choi et al. [56]

Since the feed is in a liquid form, it has to be vaporized prior to the reactions. Therefore, the reformer should include three functional units in series for feed evaporation, reforming and CPOX reactions, and gas clean-up.

1.3 Reformers for Hydrogen Supply

In recent years, many companies have conducted extensive research on fuel processors to produce hydrogen from hydrocarbon fuels (Table 1-2). These are mainly for the PEMFC for automobile application.

Table 1-2 Companies developing fuel processor technology [62-64]

Corporation	Fuel type		Primary fuel processor		CO conversion processes		Tech. status (max. capacity)
	Methanol	Gasoline	SR	POX[1]	WGS[2]	PROX[3]	
Epyx	Second	First		√	√	√	50 kW
Daimler Benz	First	Second	√			√	50 kW
GM	First	Second	√		√	√	30 kW
Honda	Sole		√			√	
HBT		Sole		√	√		7-42kW
IFC	First	Second	√	√	√	√	100 kW
JM	First	Second	√	√	√		6 kW
Mitsubishi	Sole		√		√	√	10 kW
Nissan	Sole		√		√	√	
Toyota	Sole		√		√	√	25 kW

[1]POX: Partial Oxidation Reaction [2]WGS: Water Gas Shift Reaction [3]PROX: Preferential Oxidation Reaction Epyx: an Arthur D. Little company – one of the leading developers of compact fuel processing system solutions for fuel cell applications in the micro power and transportation markets. HBT: Hydrogen Burner Technology, Inc. IFC: International Fuel Cells JM: Johnson Matthey

Although the fuel processors described in Table 1-2 are of large scale, smaller ones are also of interest for numerous practical applications. Main focus of the present study is on the small-scale compact reformers.

1.3.1 Compact Reformer for PEMFC Application

A commercially viable portable reformer requires high efficiency in terms of conversion of hydrocarbon fuel and thermal management, compactness, and easy integration with the fuel cell. Numerous researchers have been working on meeting these requirements, and the current research has been also on investigating and assessing a new design idea that satisfies all these requirements.

Patil et al. [65] presented a 40 watt methanol fuel processor which consisted of a vaporizer, steam reformer, and recuperative heat exchanger while the weight of entire system was less than 80g. Yamamoto et al. [66] reported a multi-layered micro-channel reactor which was capable of combined functions as a vaporizer, a methanol reformer, a carbon monoxide removal device, and a catalytic combustor to supply heat for the endothermic steam reforming reaction. Their micro-channel reactor was made of glass with a power generation rate of about 10W for a laptop PC. Park et al. [67] disclosed an integrated fuel cell system with a methanol fuel processor that consisted of a fuel vaporizer, heat exchanger, reformer, and catalytic combustor. Kundu et al. [68] reported a Micro-Electro-Mechanical System (MEMS)-based micro-reformer which was intended for cellular phone application. Kwon et al. [69] developed a micro-reformer using a silicon wafer as the reactor substrate based on microelectronics fabrication technology, whereas Rense et al. [70] demonstrated a micro-reformer using a thin metal plate as the reactor substrate. In the work of Reuse and coworkers, total oxidation of methanol was used to provide the heat needed for the hydrogen-generating steam reforming reaction by adopting a two-passage reactor system for the two separate reactions.

1.3.2 A Common Design Approach

Although most industrial research [71] on micro-reformers is rather secretive without much published information, it seems that one of the most popular approaches is to adopt a tubular reactor type that consists of serpentine micro-channels etched on a thin substrate such as silicon wafer (Figure 1-3). The cross section of the reactor path is a rectangular shape with its dimension in the order of hundred micrometers and the inner surface of the rectangular channels is coated with a catalyst for the steam reforming reaction. The catalysts (Cu/ZnO type for the steam reforming and Ru/Rh type for the gas clean-up both supported on alumina) are deposited on the surface along the groove by solution coating or sputtering [72, 73]. Temperature control is achieved by heating the substrate plate.

It was shown that when the grooved cross-section was about 200 by 200 micrometers with the total length of about 30 cm, hydrogen could be produced at a rate of about 1L/hr at standard condition. Because a production rate larger than 15L/hr is required for a 10W usage assuming 30-40% efficiency, many of the thin single-meander reactors need to be stacked. When the hydrocarbon fuel (e.g. methanol solution of water) is fed into the reactor inlet, the reaction occurs and generates hydrogen as the hydrocarbon fuel flows through the serpentine reactor path.

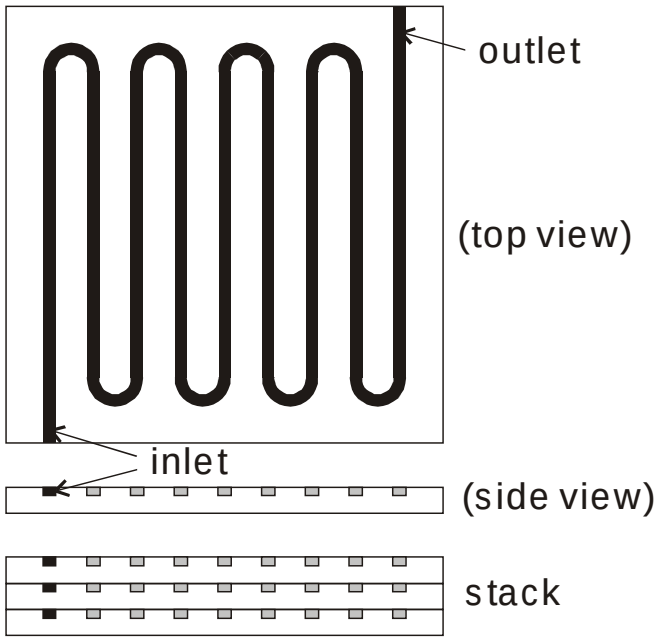

Figure 1-3 Schematic of a micro-reformer with serpentine micro channels

The reactor is typically kept at about 200~250ºC for the reaction, and heat is provided continuously from an external power source like a separate battery unit because the steam reforming reaction is endothermic. This type of approach has been demonstrated by Motorola laboratory, Casio and a few other institutions for micro-PEMFC applications. However, such reformers are only prototypes that still require breakthroughs for commercial use. Major problems or difficulties with this approach include [74-77]

1. Difficulty in catalyst incorporation and low catalyst efficiency due to small contact area
2. Difficulty in section-wise temperature control.
3. Difficulty in leak-proof stacking.
4. Difficulty in feed stream branching with uniform flow rate for each stack.
5. Difficulty in catalyst replacement after catalyst deactivation

Furthermore, because the steam reforming reaction is a gas phase reaction, the reactants should be vaporized prior to be injected into the reactor and that also requires an external energy source [78, 79]. Although it is claimed that the battery which supplies heat for the reaction can

be recharged using the energy generated by the fuel cell itself, the energy consumption for the recharging becomes a substantial portion of the energy generated by fuel cell [80-82].

In the present study a new design idea is explored that may resolve most of the difficulties described above. As it will be described in more detail in the following sections, the new design concept appears to offer various advantages as described above, and the current study is to demonstrate its viability through process modeling and experiments.

CHAPTER 2
A NEW COMPACT REFORMER

2.1 Characteristics of the Proposed Reformer

It has been described in the previous section that one of the difficulties in making a compact reformer is the difficulty in catalyst incorporation and low catalyst efficiency associated with small contact area when surface coating method is applied. One idea to increase the catalyst efficiency is the conventional tubular reactor in which granular catalyst particles are packed in cylindrical reaction channels. In order to make a reformer to be self-sustaining without an external energy source, the exothermic CPOX (reaction 1-6) may be induced along with the endothermic steam reforming reaction.

A proposed reformer design that may be capable of achieving these two requirements (i.e., improved catalyst efficiency and self-sustainability) is shown schematically in Figure 2-1. It consists of two types of basic plates; the reactor plate and the end plates (front and rear plate in Figure 2-1). The straight cylindrical channels in the reactor plate are filled with catalyst particles and the steam reforming and CPOX reactions take place in the channels. The front and the rear plates have many grooves that connect two neighboring cylindrical channels thereby changing the flow direction back and forth and forming a long meandering reaction path. The back and forth layout of channels make full utilization of space, which is necessary for the reformer to be compact enough for portable application of PEMFC.

The most important design feature of this reformer is the layout of the grooves that enable the interlacing of the flow channels. The numbers, 1 through 29, written on each cylindrical channel indicate the sequential order of the flow path through which the reactant will flow. Reactants are fed into channel #1 of the reactor through the hole (#1) in the front plate. Then they flow through the channels in the top row #2 to #10 where they are vaporized. (Although not

shown in the figure, the reformer also uses a thin film heater attached on the top surface of the reactor plate. In a complete portable fuel cell, a start-up unit (e.g. a battery) is necessary to heat up the reformer to its working temperature to allow the reactions to take place [83, 84]. The heater is to supply heat for the evaporation of methanol/water mixture and heat up the reformer to an appropriate operation temperature for the initial start-up.) The vaporized reactants then flow into channel #11 and flow sequentially from #11 to #18. The slant grooves in the end plates make these flow channels #11 through #18 to be alternating in rows and skipping immediately neighboring channels in the same row. The reactants then flow into channel #19 and sequentially from #19 through #28. Channels #19 through #28 are again alternating in rows and skipping immediately neighboring channels in the same row due to the end plate groove layout. By then, the reactions are complete and the reaction products flow through channel #29 and exit the reactor through the hole (#29) in the rear plate. We may notice that channels #11 through #18 are interlaced with the channels #19 through #28.

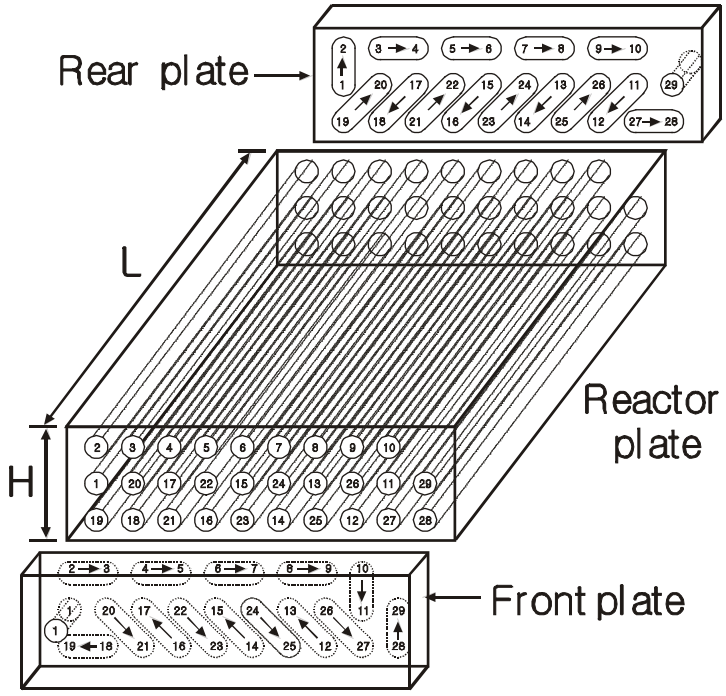

Figure 2-1 Schematic of the proposed reformer channel layout

The feed contains oxygen which is supplied from the air, and the partial oxidation reaction is dominant over the steam reforming reaction in the presence of oxygen [24, 85]. Thus, until the feed oxygen is depleted, the exothermic CPOX is the main reaction that occurs in the channels #11 through #18 where heat is generated. (We assume the CPOX reaction will be completed in the channels #11 through #18, however, it may need more or less channels for the reaction to be completed depending on the catalyst activity.) Once oxygen is depleted, only the endothermic steam reforming reaction occurs in the channels #19 through #28. Because channels #11 through #18 are interlaced with channels #19 through #28, the heat generated in #11 through #18 are transferred effectively to channels #19 through #28. This interlacing of the channels that enable efficient heat transfer may be one of the most novel features of the reformer design. Furthermore, this reformer is of a modular structure in that multiple units can be combined either vertically or horizontally depending on the required hydrogen production rate.

2.2 Determination of the Reformer Dimension

2.2.1 Flow through a Packed Channel and the Pressure Field [86, 87]

For a low Reynolds number flow, the pressure drop through a packed bed can be described by the Kozeny-Carman equation which describes the linear relationship between the pressure drop and the superficial velocity of the fluid.

$$\frac{\Delta p}{L} = \frac{150 V_0 \mu}{\Phi_s^2 D_p^2} \frac{(1-\varepsilon)^2}{\varepsilon^3} \tag{2-1}$$

Here $\frac{\Delta p}{L}$ is the pressure drop per unit length, μ is the viscosity of fluid, ε is the porosity, Φ_s is the sphericity, D_p is the characteristic length scale for the packing material, V_0 is the superficial velocity which is the volumetric flow rate divided by the cross-sectional area of the channel. This

equation is equivalent to the Darcy's law in that the average velocity (or flow rate) is proportional to the pressure gradient.

When the Reynolds number is very large, inertial force is dominant over viscous force and the pressure drop becomes proportional to the square of average velocity as described by the Burke-Plummer equation:

$$\frac{\Delta p}{L} = \frac{1.75 \rho V_0^2}{\Phi_s D_p} \frac{(1-\varepsilon)}{\varepsilon^3} \tag{2-2}$$

For a flow at a moderate Reynolds number, the Ergun equation is known to describe the relationship between the average velocity and the pressure drop. The Ergun equation is nothing but the simple addition of the Kozeny-Carman equation and the Burke-Plummer equation:

$$\frac{\Delta p}{L} = \frac{150 V_0 \mu}{\Phi_s^2 D_p^2} \frac{(1-\varepsilon)^2}{\varepsilon^3} + \frac{1.75 \rho V_0^2}{\Phi_s D_p} \frac{(1-\varepsilon)}{\varepsilon^3} \tag{2-3}$$

The Ergun equation has been used in describing the flow of current interest in which the flow is mostly gaseous and the chemical reactions described in section 1.2 are taking place.

2.2.2 Dimension of a prototype reformer

One of the design criteria that defines the size of the reformer is the hydrogen generation rate. In the present study, main focus will be on a micro-reformer that can produce a suitable amount of hydrogen for a 10W PEMFC application. Because the reactants are in gas phase, gaseous flow through a packed tube has been investigated using the Ergun equation to determine the suitable channel dimension and the size of the catalyst particles.

The Ergun equation (Equation 2-3) is for a flow of an incompressible fluid in which the fluid properties such as density and viscosity are constant. However, the reactants are in gaseous phase, and the flow of current interest is a compressible flow in which the density may change

considerably. However, if the average velocity is low so that the pressure drop is not very significant, use of Ergun equation is justified for a compressible flow. One guideline may be the Mach number (*Ma*), in that if *Ma* is much smaller than 1, incompressible flow equations can be used for compressible flow. Typically, the average velocity in the reformer is in the range of about 0.1~1 m/s. Thus, the Mach number for the flow of current interest is much smaller than 1.

In using the Ergun equation for a compressible flow, however, the density variation due to the pressure change has to be taken care of properly. In the present calculation, the Ergun equation was applied in a segment-wise manner assuming a quasi-steady state in each segment. That is

$$\frac{\Delta p_i}{\ell_i} = \frac{150 V_i \mu_i}{\Phi_s^2 D_p^2} \frac{(1-\varepsilon)^2}{\varepsilon^3} + \frac{1.75 \rho_i V_i^2}{\Phi_s D_p} \frac{(1-\varepsilon)}{\varepsilon^3} = a \mu_i V_i + b \rho_i V_i^2 \qquad (2\text{-}4)$$

where the subscript *i* indicates the small i-th segment. The physical properties μ_i and ρ_i are calculated at the average pressure in each segment, and the average velocity is calculated using the density ρ_i in that segment. The density ρ_i can be calculated once the molar flow rate of each chemical component in the gaseous stream is known. Assuming that the conversions of the chemical reactions (i.e., steam reforming and CPOX reactions) are uniform, the molar composition at each segment can be calculated.

In Figure 2-2, the molar composition inside the reformer is shown for the ideal situation. Initially it was assumed that the reformer consisted of 19 segments and that

- Only CPOX is taking place for the first half of the reaction path where oxygen is consumed, and the steam reforming reaction takes place in the second half.
- Oxygen is supplied from the air so that nitrogen is also present in the stream.
- The change in viscosity is negligibly small.

Table 2-1 Initial flow rates of all species

Species	Methanol	Water	O_2	N_2	H_2	CO_2
Initial flow rate (mol/hr)	0.102	0.046	0.028	0.112	0.00	0.00
Initial flow rate ($\times 10^{-5}$ mol/s)	2.83	1.28	0.778	3.11	0.00	0.00

Also assuming 50% efficiency of a fuel cell, the required hydrogen production rate for 10W is calculated to be 0.252 mol/h. Hydrogen is produced by both the steam reforming (SR) and the CPOX reactions. In determining the relative production rate of hydrogen by each reaction, it was assumed that the amount of heat generated by the CPOX reaction is balanced with the heat required by the SR reaction so that the reformer is self-sufficient in term of energy requirement. Assuming 100% conversion of both the partial oxidation reaction and the steam reforming reaction, the required feed flow rates of methanol, water and oxygen, to give the desired hydrogen production rate, are given in Table 2-1. For a model case, where the reaction rate is constant irrespective of the concentration of species in the reactor, the molar flow rates of all chemical species are shown in Figure 2-2.

Figure 2-2 indicates that the molar flow rate of the inert nitrogen is constant, and that the oxygen is gradually consumed and depleted in the first half. The molar flow rate of water is constant for the first half and decreases gradually to depletion in the second half where the steam reforming reaction is taking place. The hydrogen production rate in the second half is greater than that in the first half because 3 moles of hydrogen are produced per mole of methanol by the steam reforming reaction whereas 2 moles of hydrogen are produced per mole of methanol by the CPOX reaction.

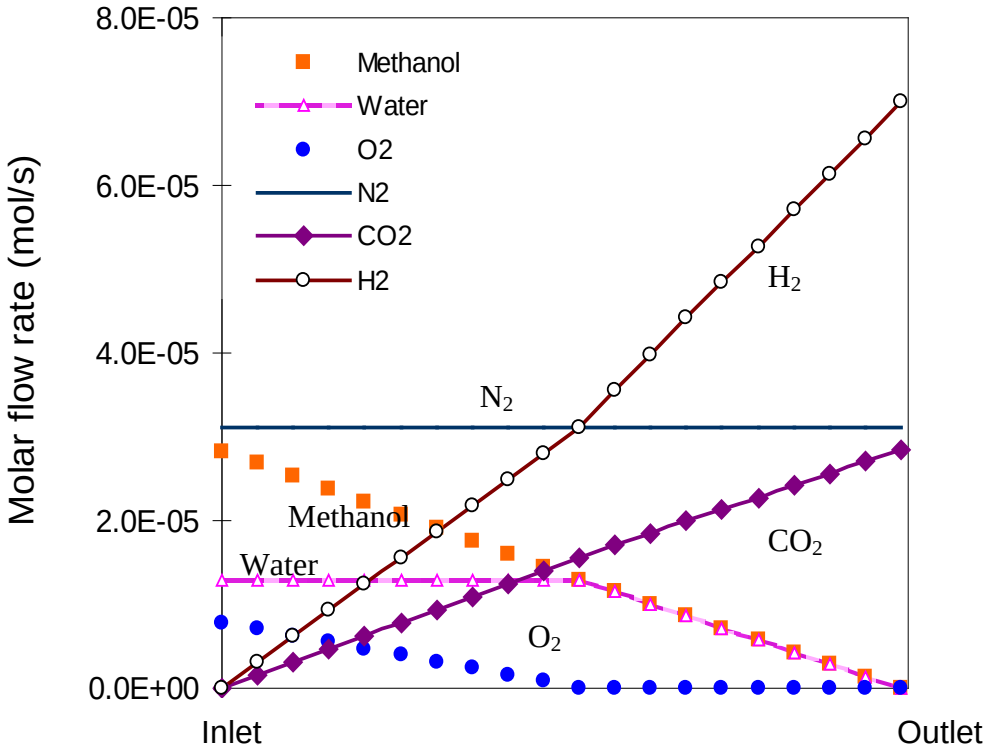

Figure 2-2 Molar flow rates of each chemical species along the flow path of the reformer (total length 95 cm)

With the component molar flow rates known, the average density and the average volumetric flow rate of the fluid in each segment can be estimated using the ideal gas law. In addition, the effective viscosity can be estimated using the following semiempirical formula of Wilke [88, 89]:

$$\mu_{mix} = \sum_{\alpha=1}^{N} \frac{x_\alpha \mu_\alpha}{\sum_\beta x_\beta \Phi_{\alpha\beta}} \tag{2-5}$$

where N is the number of chemical species in the mixture. x_α and μ_α are the mole fraction and the viscosity of species α, at the system temperature and pressure. The dimensionless parameter $\Phi_{\alpha\beta}$ is defined as:

$$\Phi_{\alpha\beta} = \frac{1}{\sqrt{8}}\left(1+\frac{M_\alpha}{M_\beta}\right)^{-1/2}\left[1+\left(\frac{\mu_\alpha}{\mu_\beta}\right)^{1/2}\left(\frac{M_\beta}{M_\alpha}\right)^{1/4}\right]^2 \quad (2\text{-}6)$$

where M_α is the molecular weight of species α. With the density, viscosity and the average velocity of the gaseous mixture in the segment known, the pressure drop can be calculated using equation (2-4) once the inlet pressure is known. However, the inlet pressure is not known *a priori*, and should be determined iteratively. However because the outlet pressure is usually known, the pressure profile can be calculated backward starting from the outlet toward the inlet.

If the mass of catalyst is the same, when the diameter of the catalyst particle becomes smaller, the accessible surface area of the catalyst will increase and be beneficial for chemical reactions taken place on the surface. In large particles the diffusion of reactants to and products from the catalyst surface can be severely limiting for the reaction. To determine the reactor dimensions and reasonable catalyst particle sizes, model calculations were carried out at varying reactor channel diameters and as a function of catalyst particle size to determine the pressure drops in each case.

Assuming the reformer channel diameter is 2.5 mm, by varying the size of the spherical catalyst particle of 150 μm, 200 μm, 250 μm and 300 μm, the pressure profile along the reformer flow path is given in Figure 2-3. These pressure profiles were determined by the backward calculation assuming that the outlet pressure is 1.5 atm.

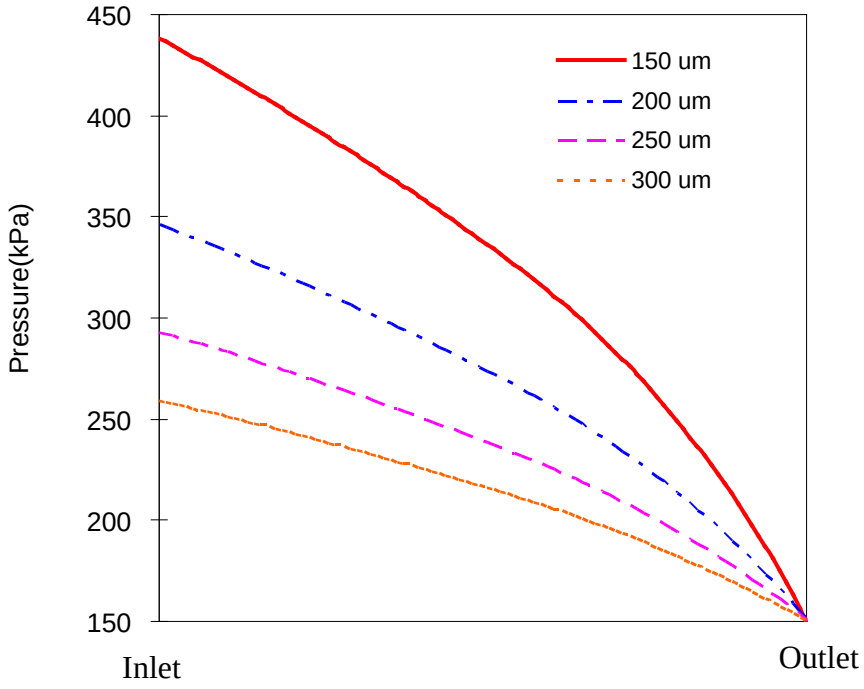

Figure 2-3 Pressure profile along the flow path at various particle size (reformer channel Dia.= 2.5 mm)

Considering that a reasonable pressure drop in the reformer is about 2~3 atm, a catalyst particle size of 150 μm would on the small side as it gives a pressure drop of close to 3 atm. It appears that a catalyst particle of about 200 μm is an appropriate size that can be used at this reformer diameter (2.5 mm). This particle size will result in an acceptable pressure drop, and it should keep the diffusion limitations at a reasonable level.

To determine an appropriate reactor diameter, for a catalyst particle size of 200 μm, the pressure profiles were determined at reactor channel diameters of 2.0 mm, 2.5 mm and 3.0 mm (see Figure 2-4).

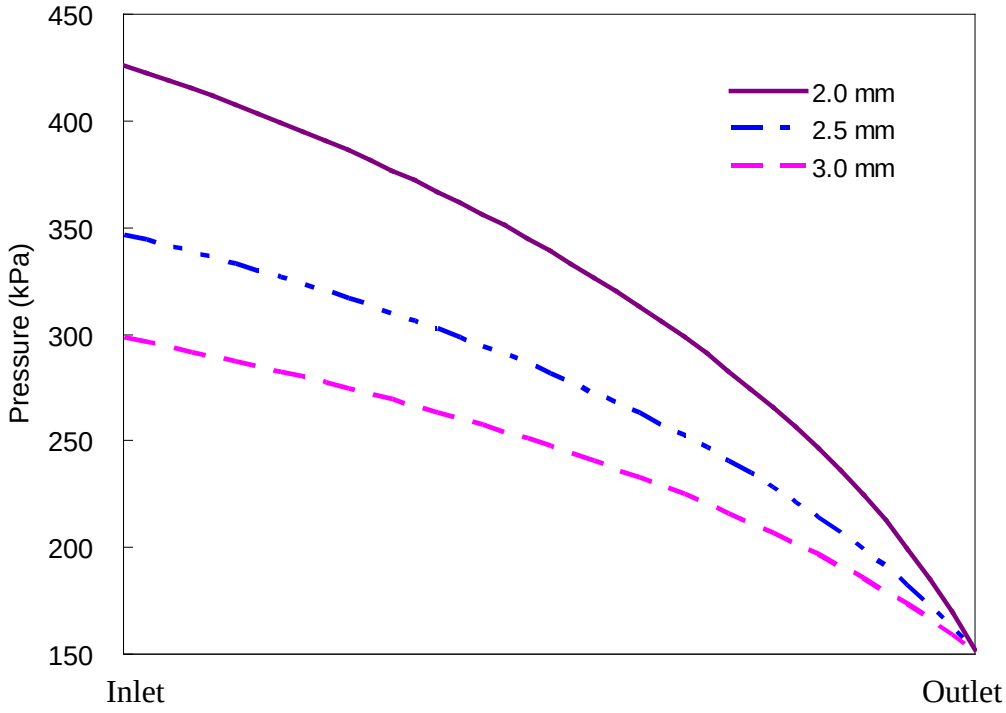

Figure 2-4 Pressure profile along the flow path

According to these calculations, a reactor channel diameter of 2.5 mm is the smallest diameter that will give a reasonable pressure drop (1-2 atm.) when using catalyst particle sizes of 200 μm. Decreasing the reactor diameter to 2.0 mm, will result in a pressure drop of close to 3 atm. Considering that these are only model calculations, it is wise to avoid the reactor and catalyst dimensions that give pressure drops close to the upper bound.

Calculation of the pressure profile using Equation (2-4) will be less accurate if the number of segments is too small. Thus, additional calculations were made by varying the number of segments from 10 to 38. The result with 19 segments was virtually the same as those with higher number of segments indicating that 19-segment calculation was appropriate without serious calculation error.

Based on the result given in Figure 2-4, the channel diameter has been determined to be 2.5mm for a prototype reformer. Its overall dimension has been chosen to be 76 x 76 x 18 mm

making the total volume of the prototype reformer to be about 104 cm^3 that seems compact enough for portable PEMFC applications. In Figure 2-5, the reformer manufactured according to this dimensional specification is shown.

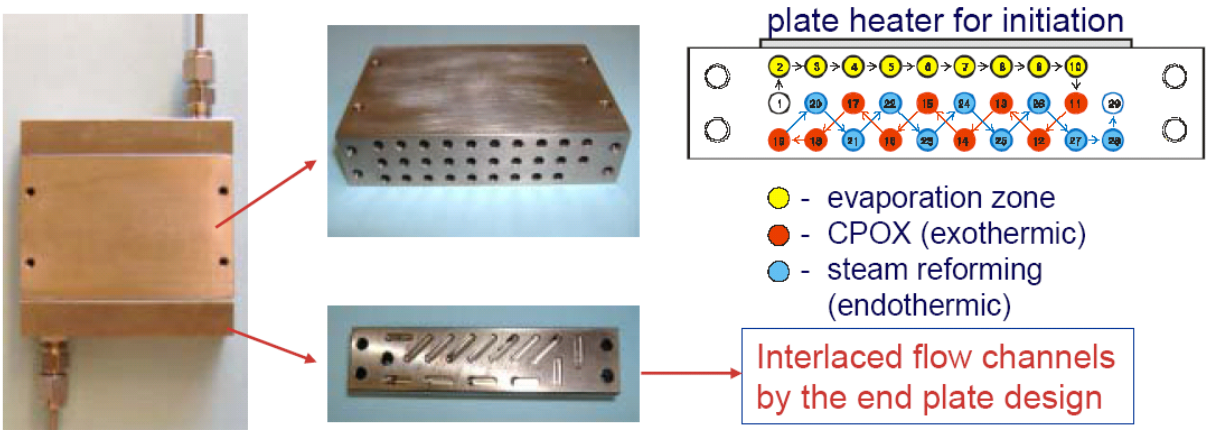

Figure 2-5 Details of the reformer body and end plate

2.2.3 Simulation with more Realistic Reaction Kinetics

In the previous section, the underlying assumption that the conversions of the chemical reactions (i.e., steam reforming and CPOX reactions) are uniform is equivalent to assuming that both reactions are zeroth-order. In this section, more realistic reaction kinetics proposed by other researchers [45, 85, 90, 91, 92] are used for the prediction of molar composition along the reformer. In the refined calculation, the following assumptions are still made

- CPOX reaction is dominant over SR reaction until oxygen is depleted.
- Oxygen is supplied from the air so that nitrogen is also present in the stream.
- The change in viscosity is negligibly small.

In 2007, Lin et al. [45] suggested the following kinetic model for the catalytic partial oxidation reaction (CPOX) over a 40 wt% Cu/ZnO catalyst prepared via the co-precipitation method.

$$r_{CPOX} = k_{CPOX}[CH_3OH][O_2] \quad (2\text{-}7)$$

Using a feed composition of O_2, CH_3OH and N_2 with O_2/CH_3OH ratio kept at 0.3, they determined a reaction rate constant, k_{CPOX}, of 13388 L^2/mol-s-g_{cat} at 200ºC. Here g_{cat} is weight of the catalyst in grams.

For the steam-reforming (SR) reaction, the following reaction kinetics over a commercial catalyst (BASF [S3-85]; consisting of 31.7% CuO, 49.5% ZnO and 18.8% Al_2O_3) has been suggested by Jiang et al. in 1993: [90, 91].

$$r_{SR} = k_{SR} P_{CH_3OH}^{0.26} P_{H_2O}^{0.03} \quad (P_{H_2} < 7kPa) \quad (2\text{-}8)$$

$$r_{SR} = k_{SR} P_{CH_3OH}^{0.26} P_{H_2O}^{0.03} P_{H_2}^{-0.2} \quad (P_{H_2} > 7kPa) \quad (2\text{-}9)$$

Since CPOX reaction is assumed to occur prior to the SR reaction, there will be hydrogen in the reaction by the time SR reaction takes place. As it will be shown, the hydrogen partial pressure is always larger than 7 kPa when SR reaction occurs. Thus, only the 2nd kinetic expression [i.e., eqn (2-9)] is used in the calculations. According to Agrell et al. [85] in 2002, the reaction rate constant for this reaction is 1.37×10^{-5} mol/s-g_{cat}-$kPa^{0.09}$ at 200ºC.

Apparently, the reaction rate constant for the CPOX reaction is many orders of magnitude larger than that for the SR reaction. Thus, the CPOX reaction is expected to be an extremely fast reaction that may take place within a very short distance from the inlet to the reformer. However, as it will be shown in later chapter, it is likely that the CPOX reaction does not occur as fast over the catalyst with the proposed experimental conditions in the actual reformer. Also, this is not necessarily detrimental to the operation of the reformer, as the catalyst can be diluted with inert material to reduce the reaction rate in the CPOX portion of the reforming.

In a differential segment (or element) of an ideal tubular reactor (or a plug-flow reactor), the material balance for a reactant A (e.g., methanol) is given as

$$dN_A = r_A dV = r_A A dx \tag{2-10}$$

Here dN_A (mol/s) is the rate of increase of species A within the differential element of the reactor, r_A is the production rate of A per unit volume of the reactor (i.e., mol/s-L), and dV is the differential volume of the reactor (L) which is the product of the cross-sectional area (A) and the differential length (dx) of the reactor. Thus, for the CPOX reaction, the molar rate of change of methanol is given as

$$\frac{dN_{MeOH}}{dx} = k_{CPOX}[CH_3OH][O_2] \cdot A \tag{2-11}$$

Once the reformer volume and the amount of the catalyst in the reformer are known, the reaction rate constant is known. Assuming idea gas law, the molar volume of the reactant mixture can be calculated if the absolute pressure at the given reactor position is known. Hence the volumetric concentration of each reactant can be calculated.

The numerical calculation has been performed following the procedure described below:

1) Assume the inlet pressure and calculate the initial volumetric concentration of the reactants for a given feed rate of the reactants, see Table 2-1.
2) Calculate the molar rate of change of methanol for a small segmental length of the reactor (e.g., $dx = 10^{-5}$ cm) assuming that only CPOX reaction takes place in the beginning.
3) Determine molar rates of change for all other species using the reaction stoichiometry.
4) Calculate the pressure drop through the differential segment of the reactor and update the pressure at the down-stream position and the molar concentration of all chemical species.
5) March forward following the same scheme until oxygen is depleted (i.e., more than 99.9% oxygen is consumed).

6) Apply the same calculation scheme but using the kinetic expression for the SR reaction through the remaining length of the reformer.

7) If the exit pressure is different from the target value (e.g., 1.5 atm), assume a new value for the inlet pressure and repeat the entire calculation procedure.

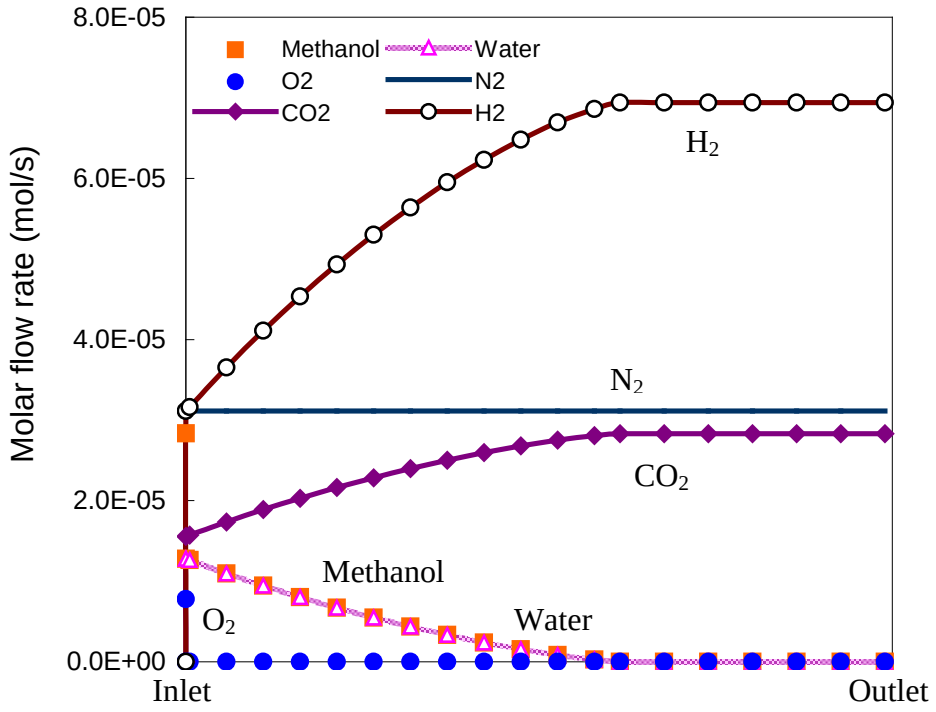

Figure 2-6 Molar flow rates of each chemical species along the flow path of the reformer calculated for k_{CPOX} = 13388 L2/mol-s-gcat and k_{SR} = 1.37×10-5 mol/s-gcat-kPa$^{0.09}$

Following the procedure given above, calculations were conducted for several different values of the reaction rate constants and the results are shown in Figures 2-6 through 2-11 in the same format as Figure 2-2. All results were obtained for a reformer whose diameter is 2.5 mm with the total length of 95 cm. If it is not specified specially, the x-axis represents total flow path of reformer (95cm). The total weight of catalyst in the reformer was assumed to be 2 grams, which in fact is the actual amount for the experiment that will be described in the later sections.

The reactant feed rates were 2.83×10^{-5}, 1.28×10^{-5} and 3.89×10^{-5} mol/s for methanol, water and air, respectively (as given in Table 2-1).

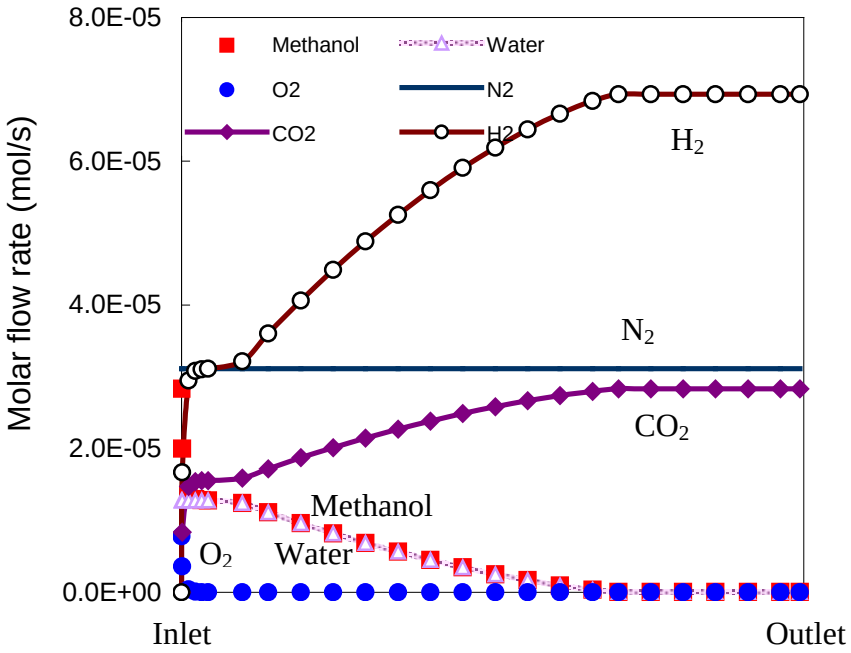

Figure 2-7 Molar flow rates of each chemical species along the flow path of the reformer calculated for k_{CPOX} = 13.388 L^2/mol-s-g_{cat} and k_{SR} = 1.37×10^{-5} mol/s-g_{cat}-$kPa^{0.09}$

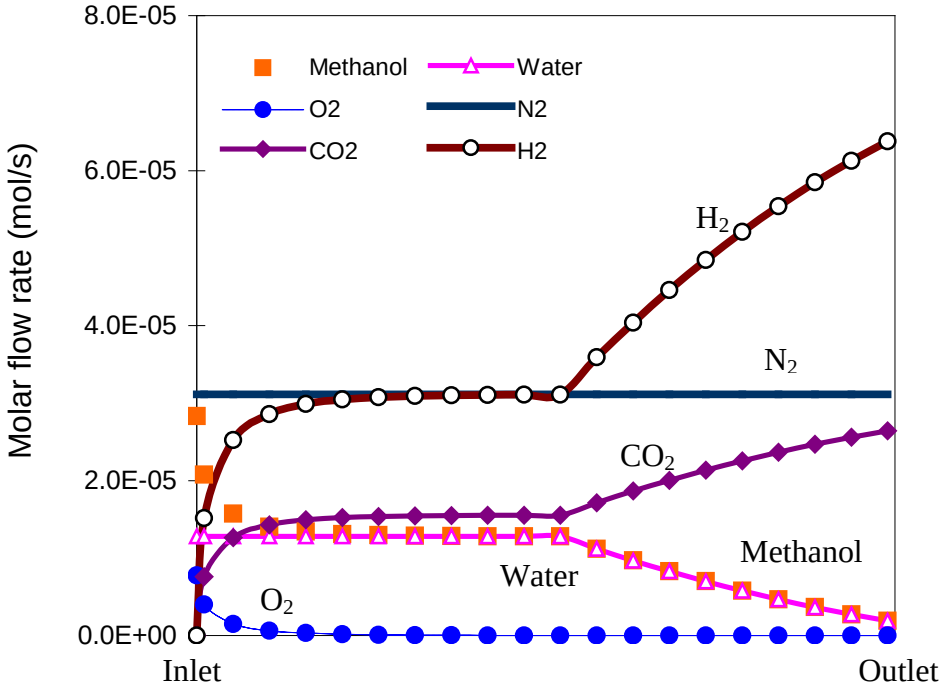

Figure 2-8 Molar flow rates of each chemical species along the flow path of the reformer calculated for k_{CPOX} = 1.3388 L^2/mol-s-g_{cat} and k_{SR} = 1.37×10^{-5} mol/s-g_{cat}-$kPa^{0.09}$

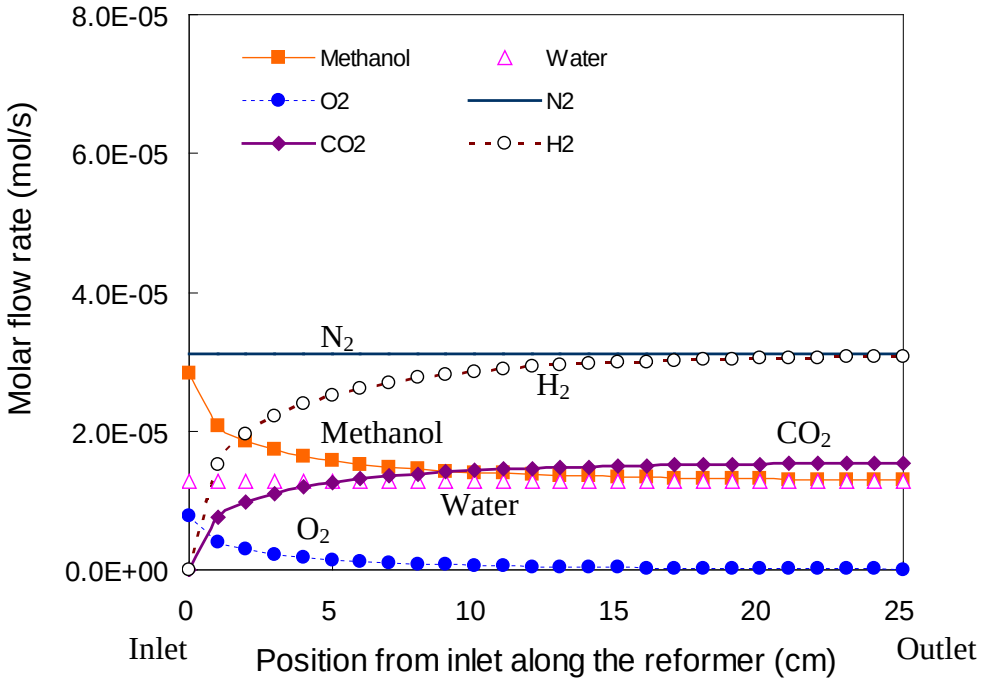

Figure 2-9 Molar flow rates of each chemical species along the flow path of the reformer calculated for the same values of k_{CPOX} and k_{SR} for Figure 2-8, but for a small reformer length near the inlet to show the fast decline of oxygen

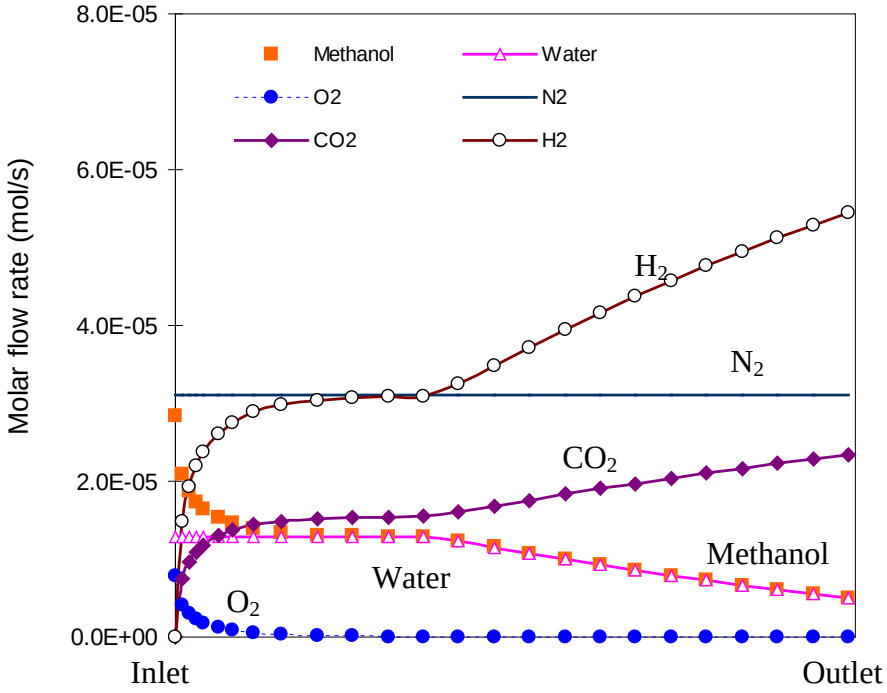

Figure 2-10 Molar flow rates of each chemical species along the flow path of the reformer calculated for k_{CPOX} = 1.3388 L^2/mol-s-g_{cat} and k_{SR} =6.85×10^{-6} mol/s-g_{cat}-$kPa^{0.09}$ to show the influence of slower reaction kinetics for the SR rxn.

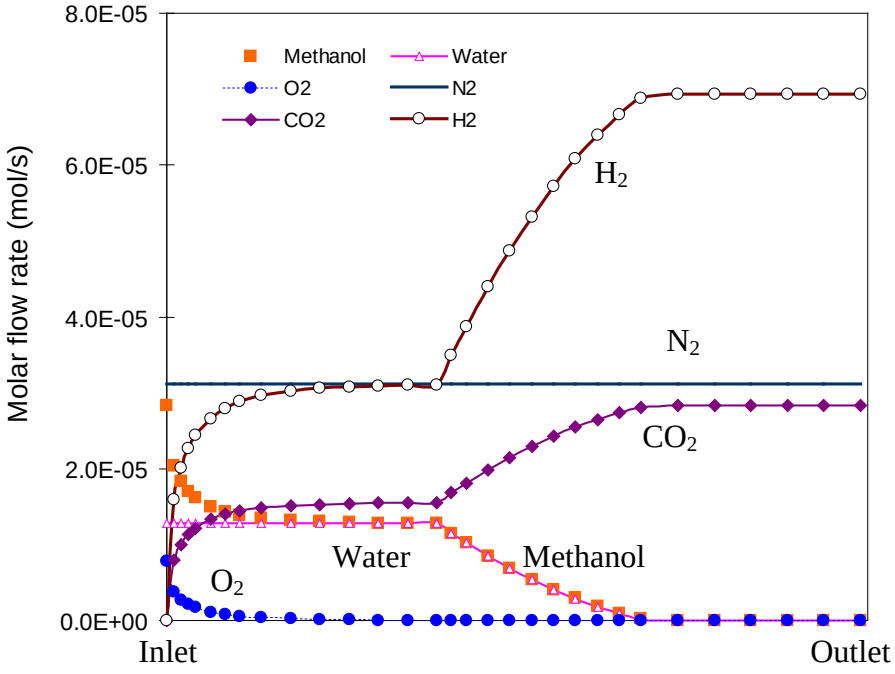

Figure 2-11 Molar flow rates of each chemical species along the flow path of the reformer calculated for k_{CPOX} = 1.3388 L^2/mol-s-g_{cat} and k_{SR} =2.74×10^{-5} mol/s-g_{cat}-$kPa^{0.09}$ to show faster reaction kinetics for the SR rxn.

As Figure 2-6 indicates, if the reaction rate constant for the CPOX reaction is as large as suggested by Lin et al. (2007), the reaction is extremely fast and occurs within an unreasonably short length. For this large rate constant, the molar rate of change of both methanol and oxygen is very steep and consequently, the numerical calculation is likely to not be very accurate unless an extremely short segment length is used. When the reaction rate constant for the CPOX reaction is much smaller, its reaction length increases as Figures 2-7 through 2-9 indicate. Similarly, the reformer length for the SR reaction increases if the reaction rate constant gets smaller (Figure 2-10), whereas it decreases if the reaction rate constant is larger (Figure 2-11).

As the pressure profiles for the reformer design were based on the model calculations given in Figure 2-2, these pressure profiles were recalculated for the reaction conditions in Figures 2-7 and 2-11 (see Figures 2-12 and 2-13).

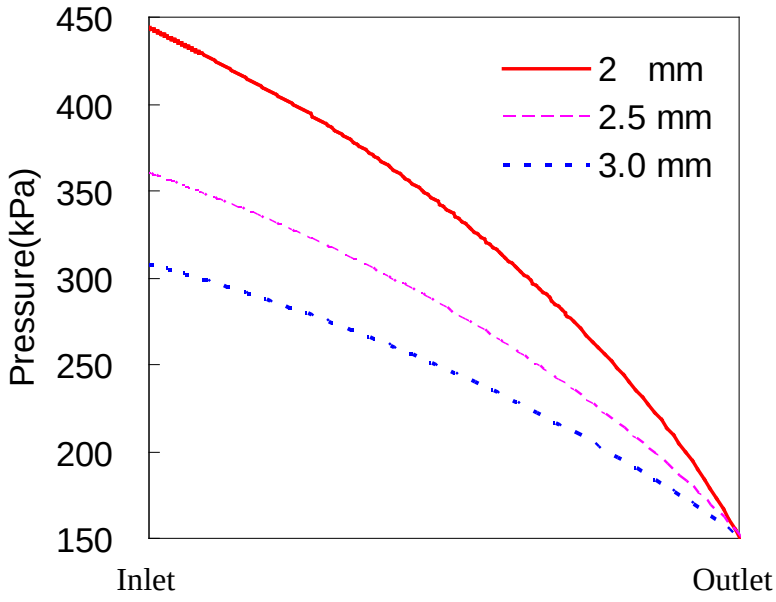

Figure 2-12 Pressure profile along the flow path based on the reaction conditions for Figure 2-7

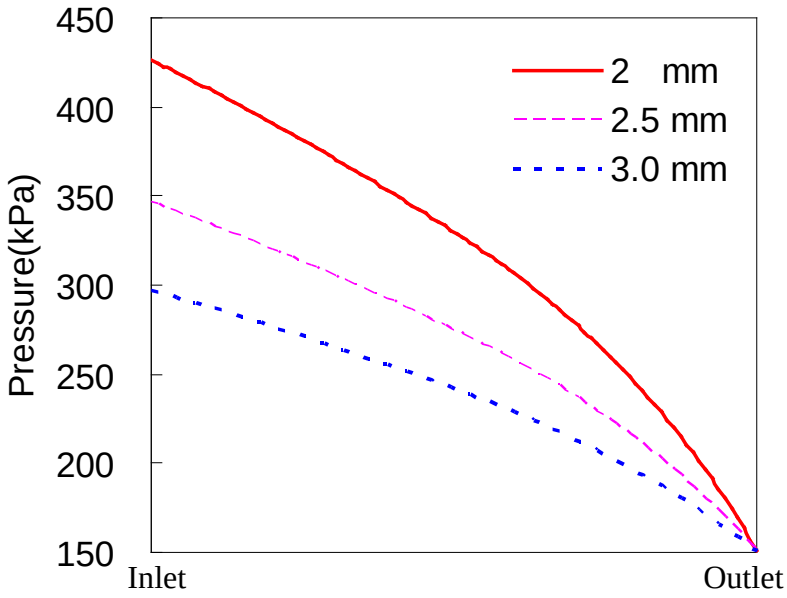

Figure 2-13 Pressure profile along the flow path based on the reaction conditions for Figure 2-11

As is evident in Figures 2-12 and 2-13, these pressure profiles are not much different from those in Figure 2-4. These calculations suggest that the pressure profiles obtained under very simplified conditions can give reasonable results, even though the composition along the reactor may be rather unrealistic.

CHAPTER 3
EXPERIMENTAL STUDY

3.1 Experimental Setup

Figure 3-1 shows the experimental setup schematically. The main components of the setup are (1) an air compressor to supply oxygen to the reformer along with nitrogen, (2) syringe pump to supply methanol/water liquid mixture, (3) the compact reformer shown in Figure 2-5, and (4) the temperature controller to control the operating temperature of the reformer and (5) a cold trap is located at the outlet of the reformer to condense any unreacted methanol and water from the feed. There are three pressure gauges to monitor the pressure at three different locations. The flow meters are both small volume rotameters that are used to monitor the flow rate of the air or the total product flow rate. The temperature of the reformer is measured and controlled by a thermocouple attached to the surface of the reformer. Because the capacity of the heater (100 W) was rather large and the thermocouple had to be positioned just below the heater (i.e., between the heater and the top surface of the reformer), a temperature overshoot of 4~5°C was realized whenever the heater was turned on.

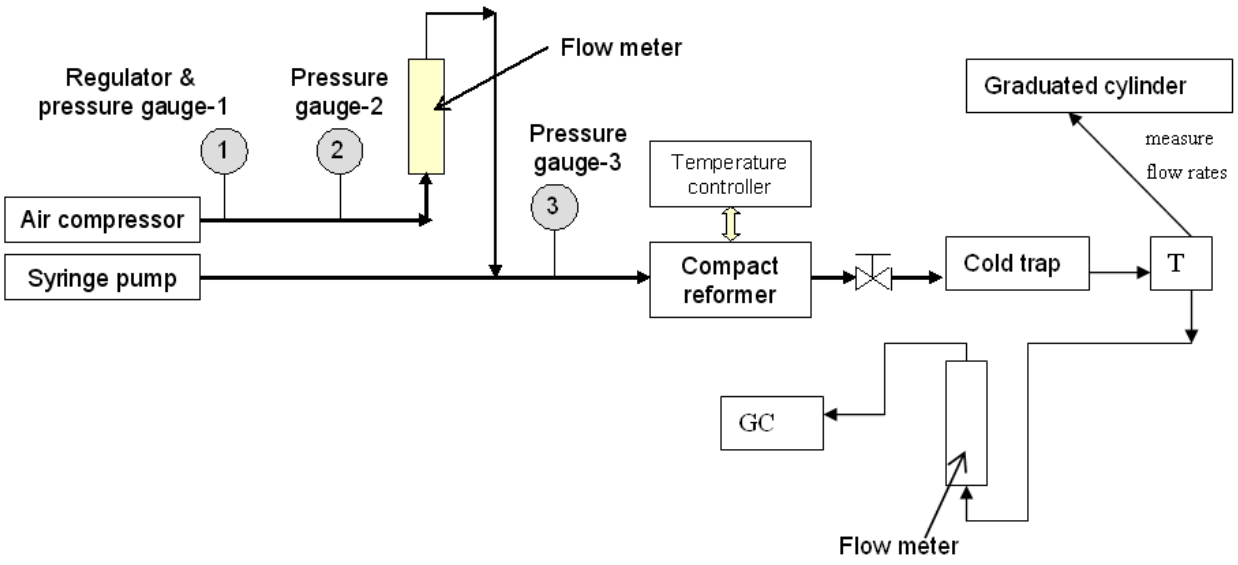

Figure 3-1 Schematic of the experimental setup

The syringe pump is driven by a stepper motor that is controlled by a PC to provide a tight control of the feed rate of the liquid phase reactants (i.e., methanol/water mixture). The flow rate of the gas phase reactant (i.e., oxygen) is more difficult to control especially when the flow rate is low as in the present case. In the current study, oxygen was supplied in the form of air stored in the tank of an air compressor. As the molar flow rate of air varies widely depending on the pressure and the temperature, calibration curves have obtained prior to the actual experiment. Details of the air flow calibration curves will be discussed in a later section. The valve at the outlet side of the reformer is to control the pressure at position 3 (i.e., the location where the pressure gauge 3 is present) in calibrating the air flow rate. This valve was wide open when the actual experiment was performed to assess the performance of the reformer. The pressure gauges 1 and 2 are analog type whereas pressure gauge 3 was a digital one.

3.1.1 Calibration of the Oxygen Feed Rate

Because the syringe pump is a positive displacement device, the feed rate of the liquid phase reactants is not determined by the system pressure but by the linear velocity of the piston. In contrast, the flow rate of the gas phase reactant (i.e., oxygen) fed from a compressed air tank depends significantly on the system pressure. Thus, the flow meter shown schematically in Figure 3-1 was calibrated prior to the experiment.

As mentioned, there were 3 pressure gauges in the experimental setup (Figure 3-1). Gauge-1 was the one attached to the regulator that controlled the pressure at the outlet of the compressed air tank of the compressor, and gauge-2 was the one measuring the pressure at the inlet to the flow meter. The experiments described later in section 3.3.2 indicated that the typical pressure at the inlet to the reformer (i.e., pressure at gauge-3 in Figure 3-1) was about 20 ~ 25 psi for the typical range of feed rates and the weight of catalyst used. Thus, in calibrating the flow

meter, the pressure at location 3 was varied between 15 to 30 psi whereas the pressure at the outlet from the tank was between 30 and 35 psi depending on the air flow rate. The choice of the pressure at location 1 (i.e., gauge-1 pressure, P_1) may be rather arbitrary as long as it is set at a value higher than the pressure at location 3. However, the higher the pressure at location 1 is, the more difficult it is to control the air flow rate. Thus, P_1 was set at a value as low as possible as long as a desired stable air flow rate was achieved.

There were two needle valves to control the air flow rate; one attached to the flow meter itself and the other located at the outlet from the reformer (Figure 3-1). From the stoichiometric equation for the CPOX reaction (Equation 1-6) and the equations (3-1) and (3-2), the standard oxygen flow rate is Y/4. That is 0.028 mol/h. Thus, the air flow rate is 0.133 mol/h or 49.8 ml/min at the standard condition. Because the air flow rate is so low, the pressure drop through the tubing from the air tank to the flow meter is as low as 1~2 psi. Thus, the pressure reading at location 2 (i.e., P_2) was between 28 and 34 psi. The pressure at the location 3 (i.e., P_3) can be controlled by the two valves. However, the valve attached to the flow meter can provide only minor adjustment whereas the valve at the outlet of the reformer (Figure 3-1) is the main control valve to adjust P_3. Thus, the calibration procedure for the air flow rate is as follows:

1) The syringe pump is shut down so that no liquid enters the system throughout the calibration procedure.
2) The pressure gauge-1 is set at 30~35 psi by adjusting the regulator knob of the compressed air tank while the valve at the reformer outlet is close.
3) Open the valve of the flow meter (i.e., rotameter) to a certain extent and gradually open the valve at the reformer outlet so that the pressure reading at location 3 (i.e., P_3) is at a desired value between 12 and 29 psi as shown in Figure 3-2.
4) Adjust the valve of the flow meter so that the float (a stainless steel ball) of the rotameter is positioned at a desired location from 2 through 5 of the rotameter indicator.
5) Measure the volumetric flow rate of the air at the exit for each float position as a function of the pressure at location 3 (between 15-30 psi).

A graduated cylinder filled with water was connected to the outlet from the reformer so that the air exiting the system displaces the water in the graduated cylinder. Thus, the displaced volume of the water per unit time is equivalent to the air flow rate.

In Figure 3-2, the measured air flow rates are given for various values of the pressure at location 3 (i.e., pressure gauge-3 in Figure 3-1). Also given in Figure 3-2 are the linear regression lines for each value of the float position.

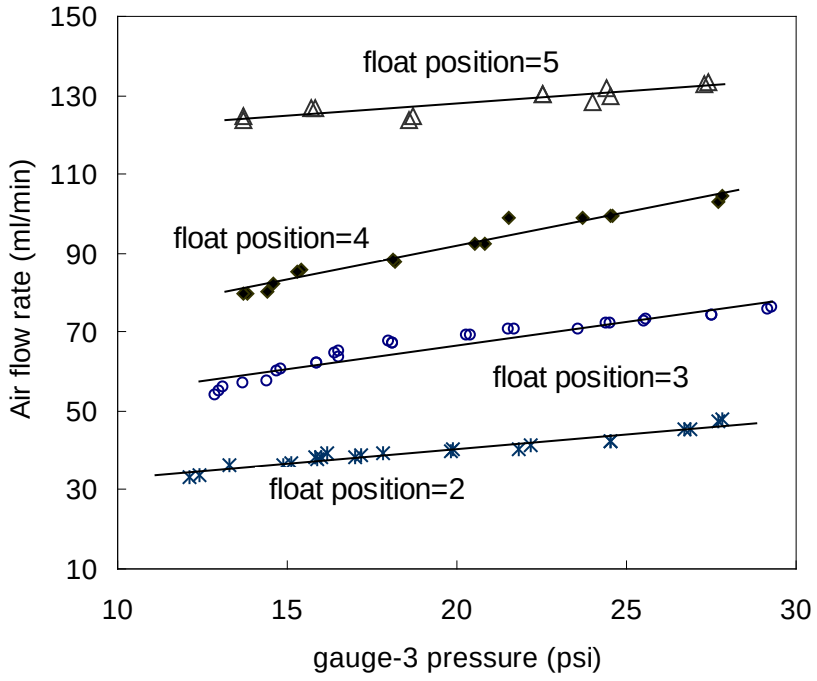

Figure 3-2 Air flow rate at various values of the pressure at location 3.

The correlation coefficients for all these lines except for float position 5 are greater than 0.9, and the following equations for the linear regression lines were used to calculate the air flow rates for the experiments described in the following section:

Float position 2: $Y = 0.747\ X + 25.515$ ($R^2 = 0.94$)

Float position 3: $Y = 1.207\ X + 42.569$ ($R^2 = 0.91$)

Float position 4: $Y = 1.724\ X + 57.342$ ($R^2 = 0.96$)

Float position 5: $Y = 0.590\ X + 116.58$ ($R^2 = 0.89$)

3.1.2 Conditions for Steam Reforming with Oxygen

The oxygen in the feed is to induce the exothermic CPOX (catalytic partial oxidation) reaction in addition to the endothermic SR (steam reforming) reaction so that the heat generated by the CPOX reaction can be used for the SR reaction for self-sustainability of the reformer.

SR reaction: $CH_3OH + H_2O \longrightarrow CO_2 + 3H_2$ (ΔH_0 = 130.9 kJ/mol) (1-3)

CPOX reaction: $CH_3OH + ½\ O_2 \longrightarrow CO_2 + 2H_2$ (ΔH_0 = -154.9 kJ/mol) (1-6)

Thus, more methanol is needed than water because methanol is consumed by both the CPOX and the SR reactions. For an ideal case in which no side reaction such as the reverse shift reaction occurs, the methanol-to-water ratio of the feed mixture can be determined for the condition that the amount of heat generated by the CPOX reaction balances with the heat needed for the steam reforming reaction. For this calcuation, the heat of reaction has to be determined first for a situation where all reactants are at room temperature (i.e., 25°C) and the product gas is at the reaction temperature (e.g., 250°C). Using appropriate thermodynamic property data for all species involved in the reations, the heats of reactions are calculated to be ΔH_{SR} = 159.8 kJ/mol and ΔH_{CPOX} = –132.5 kJ/mol, respectively. Methanol and water in the feed are in liquid phase at 25°C and the oxygen is gaseous at 25°C. Details of the calculation for the heats of reactions are given in the Appendix.

For a PEMFC with a power generation rate of 10 Watt, (or 72 kJ/h) operating at the efficiency of 50%, the hydrogen feed rate of 0.252 mol/h is needed. Thus, the reformer should be able to produce hydrogen at that rate and should be self-sustaining. These constraints can be expressed as the following set of algebraic equations:

$$X + Y = 0.252 \quad (3\text{-}1)$$

$$(159.8/3)X + (-132.5/2)Y = 0 \quad (3\text{-}2)$$

Here X and Y are the numbers of moles produced by the steam reforming (SR) and the catalytic partial oxidation (CPOX) reactions, respectively. Equation 3-1 is for the hydrogen production rate of 0.252 mol/h whereas equation 3-2 describes the energy balance for self-sustainability. The solution to these equations are X = 0.139 and Y = 0.112. Thus, the feed rates of water and methanol should be X/3 and (X/3+Y/2), respectively. That is, 0.046 and 0.102 mol/h for water and methanol, respectively. Therefore, the methanol-to-water ratio of the liquid phase feed should be 2.2 for the ideal case where the heat realeased in the partial oxidation reaction equals the heat required for the steam reforming reaction. For all experiments that followed, the liquid phase feed were the methanol/water mixture with the mixing ratio of 2.2.

3.1.3 Calibration of Product Gas Flow Rate

The product gas flow rate was measured either by the volume displacement method (as for the air calibration measurements) or via a calibrated flow meter connected to the system after the condenser. The flow meter was necessary to determine the product gas flow rate when the reformer outlet (after the condenser) was connected to the gas chromatograph (GC) for online product gas composition analysis. In this case, the volume displacement method could not be used at the same time the as composition was monitored using the GC. Thus, a second flow meter (100-500 ml/min range) was attached to the outlet of reformer after the condenser (Figure 3-1). The outlet of flow meter was then connected to the gas chromatograph. The calibration curve of the flow meter is given in Figure 3-3. The gas composition used for the calibration was approximately 20% CO_2, 50% H_2 and 30% N_2, which is similar to the composition of product gas. The calibration was done by volume displacement method.

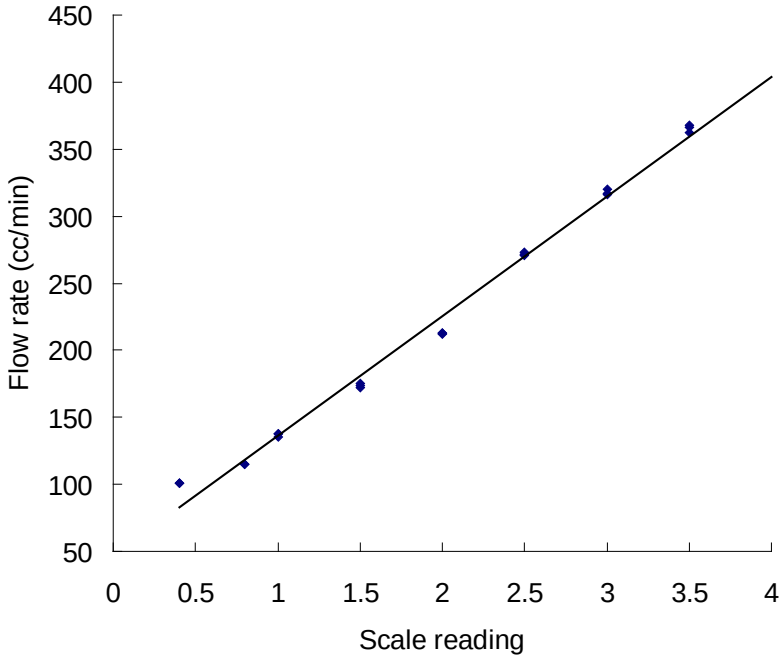

Figure 3-3 Calibration curve for 500 cc flow meter.

3.1.4 Gas Chromatography Configuration and Operation Processes

The product gas compositions were measured by a customized Agilent 6890 gas chromatograph (GC). The GC is programmed to take sample with a given volume (e.g 1.0 ml) through an automatic sampling valve. The samples can be taken either offline by manually injecting samples using a gas sampling bag or online by connecting the outlet of the steam reformer, after the condenser, to the inlet of the GC. To avoid introducing additional uncertainties in the measurements, online gas monitoring is preferred. This is particularly the case when hydrogen is a significant portion of the product stream, since hydrogen is challenging to contain.

The GC has two columns and two detectors in series. The first column is a polar Porapak Q capillary column, which separates CO_2, methanol and water. The second one is a molecular sieve column that separates the permanent gases H_2, O_2, N_2, CO. A column separation valve is

located between the columns to avoid contaminating the molecular sieve column. The first detector is a thermal conductivity detector (TCD) and the output from this detector is sent to the flame ionization detector (FID). As the FID can only detect any species containing C-H bonds (e.g. methanol and potentially methane in our case), a methanizer is placed in between the TCD and the FID. The methanizer will reduce CO and CO_2 to methane, which will allow detection with the FID and this also increases the sensitivity to these species. Lines of hydrogen, air and nitrogen are supplied to the GC and serve as the fuel, oxidant and make up gas for the FID, respectively. Only helium is supplied to the TCD and it serves as both reference and carrier gas for the TCD. The TCD can detect all chemical species in the product stream, including those detected by FID. However, the sensitivity to hydrogen is relatively low due to the He reference and carrier gas. As the concentration of hydrogen in the product stream is high, this is not a serious limitation in the experiments. Consequently, the TCD can perform all the measurements alone, but the additional FID detector provides better sensitivity for the hydrocarbon species and the CO and CO_2 due to the methanizer.

To start the GC measurements, the FID temperature is set at 400°C. It takes about 10 minutes to reach this temperature. After that, the hydrogen flame is turned on via the GC digital panel manually for the FID. The hydrogen, air and nitrogen (make-up gas) flow rates are preset to be 40, 450 and 6 sccm. The TCD temperature is maintained at 250 C and helium is used as the reference gas. The reference Helium flow is set at 33 sccm and the make-up Helium flow is set at 4 sccm. Although it is possible to control most things via the Cerity 3.0 software, it is easier to turn on the FID flame manually before starting the software. A method created in the Cerity software is then used to control the sample injection valve, the oven temperature as well as the temperatures of and flow rates in the other units (valves, columns, detectors) in the GC. With the

temperature program used, each sample takes about thirty minutes to complete. Multiple runs are taken for each sample to ensure reliable and reproducible measurements.

After completion, the collected GC data is analyzed directly by Cerity 3.0. The software will calculate the areas under the peaks in the GC spectra and this area is proportional to the concentration of the species giving rise to that peak. To be able to quantify the concentrations of each species, calibration curves with known compositions of each compound are created. The calibrations in this case had been prepared for another project using argon at a constant flow rate as an internal standard. The response (area under the peak) of each compound was plotted against the concentration of the compound. The resulting linear regression equations for CO, CO_2 and H_2 are given by the following equations:

$$CO\% = 0003*FID(CO)+0.0642 \quad (3\text{-}3)$$

$$CO_2\% = 0.0051*TCD(CO_2) + 0.3543 \quad (3\text{-}4)$$

$$H_2\% = 19.744* TCD(H_2) - 48.452 \quad (3\text{-}5)$$

FID(CO) represents integral area under the peak at the retention time for CO resulting from the FID detector, and the TCD(CO_2) and TCD(H_2) represent integral area under the peak at the retention time for CO_2 and H_2 on the TCD channel.

3.2 Experiments with Glass Bead as the Packing Material

In order to confirm the flow simulation results described in the previous chapter, experiments were performed with the reformer filled with glass bead to suppress any chemical reaction even at an elevated temperature. Because the channels 1 through 10 (Figure 2-1) of the reformer were intended to be the evaporation zone, these channels were kept empty whereas

channels 11 through 29 were packed with spherical glass bead of a diameter in the range of 177~250 μm.

For this experiment, only the liquid phase reactants were fed into the reformer with the air compressor shut off and the flow-regulating knob of the rotameter closed. The reformer was maintained at 220ºC by a thin electrical heater mounted on top of the reformer. The liquid phase reactants entering the reformer would evaporate in the evaporation zone and the gaseous feed would then flow through the packed zone before exiting to the atmosphere through the exit at the end of channel 29. The overall pressure drop for the flow was monitored by the pressure gauge-3 in Figure 3-1. Three different types of feed were used for this experiment; pure methanol, pure water, and equimolar mixture of the two. The feed rate was varied from 0.1 to 1.1 mol/h. The experiment was run for at least 10 to 15 minutes prior to taking any data (i.e., the pressure reading) to ensure steady state operation.

The experimental results are shown in Figure 3-4 along with the theoretical predictions for three different sizes of the packing material. The theoretical estimates are for a monodispersed packing material whereas the experimental results are for a polydispersed packing. Considering that the size of the glass bead is between 177 and 250 μm, the agreement between the calculated and the measured values seems reasonably good.

It is noted that the experimental results for three different types of feed form a single curve indicating that the pressure profile depends only on the total flow rate but not on the materials themselves. This result should be true only if the viscosities of the materials in gas phase are similar to each other. In estimating the pressure drop using the Ergun equation (Equation 2-4), the effective viscosity of the mixture was used as estimated by the semi-empirical relation (Equation 2-5). It should noted, however, that the effective viscosity is rather insensitive to the

composition of the gas-phase mixture, and using the viscosity of the major component in the mixture as the representative value is, in fact, sufficient in using Equation (2-4).

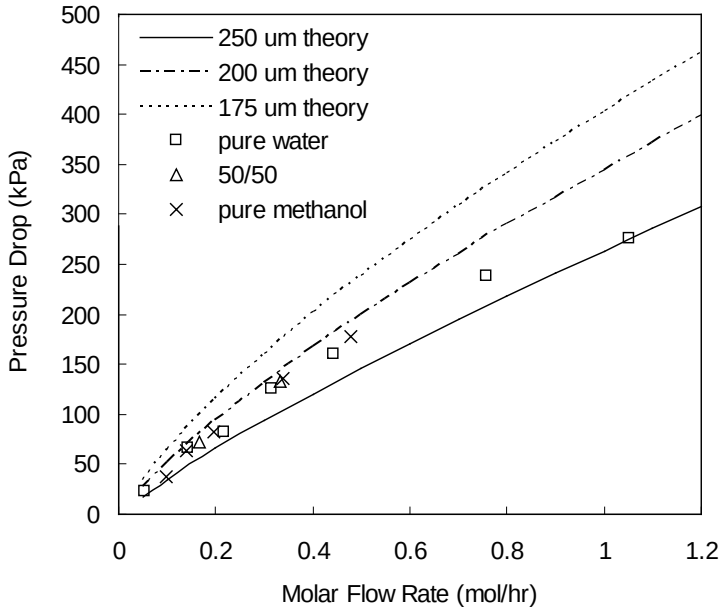

Figure 3-4 Comparison between predicted and measured pressure drop

3.3 Experiments with Cu/ZnO Catalyst

All catalyst experiment was conducted using a commercial catalyst, MDC-3, from Süd-Chemie Co. Ltd. This catalyst consists of 42% CuO, 47% ZnO, and 10% Al_2O_3, and is in a cylindrical pellet form (3.2×3.2 mm). The reaction temperature recommended by the manufacturer is between 220 and 270℃. The catalyst pellets were granulated using a ball mill and the particles in the range of 180 and 212 μm were collected using a stack of sieves. As it was described in section 3.2, the reformer channels 11 through 29 were filled with the catalyst particles, and experiments were conducted for various feed rates and compositions at a fixed reaction temperature of 220ºC which is the lowest temperature recommended for the catalyst. Some experiments were also carried out at 250ºC to determine the influence of the reformer

temperature and in one set of experiments, only the last five channels (channels 25 through 29) were filled with catalyst.

3.3.1 Steam Reforming Experiments

3.3.1.1 Low temperature experiment

In the steam reforming experiments, the feed was initially an equimolar mixture of methanol and water, and later the methanol to water molar ratio was varied to 1:2 and 1:3. In the absence of oxygen in the feed, only the steam reforming reaction would take place and the reaction temperature had to be maintained solely by the electrical heater throughout the experiment. Although reduction of the catalyst prior to the experiment is recommended for activation of the catalyst, it was bypassed as prereduction would be difficult in a truly portable reformer. Furthermore, under autothermal conditions, the oxygen added for the partial oxidation reaction would reoxidize at least part of the catalyst, which would decrease the effects of prereduction. In addition, the hydrogen produced by the steam reforming reaction itself is expected to reduce the catalyst, which may cause an induction period in which more H_2O and less H_2 is formed. For this reason, once the reformer was filled with newly prepared catalyst, experiment was conducted initially at a low feed rate of about 0.1 mol/h for approximately 12 hrs before initiating the experiments and increasing the feed rate to higher values.

For each experiment, the volumetric flow rate of the product gas exiting the reformer was measured, and samples were taken using gas sampling bags for analysis. The product gas composition measured using gas chromatography (Agilent 6800) is shown in Table 3-1 for 5 different samples. The samples 1 through 3 were taken from three different experiments conducted using the same catalyst (catalyst-1) at the same temperature (220ºC) but at different

feed rates. Experiments for samples 4 and 5 were also conducted at the same temperature of 220ºC but using a different batch of catalyst (catalyst-2).

Table 3-1 Product gas composition as a function of feed rate at steam reforming conditions (reaction temperature: 220ºC, water to methanol molar ratio=1:1)

Experiment #	1	2	3	4	5
Catalyst type	Cat.-1	Cat.-1	Cat.-1	Cat.-2	Cat.-2
Feed rate (mol/hr)	0.05	0.07	0.1	0.4	0.9
Product gas flow rate (mol/hr)	0.095	0.127	0.18	0.45	0.54
Methanol conversion	95%	91%	90%	56%	30%
H_2	76%	73%	80%	78%	77%
CO_2	20%	23%	17%	18%	21%
CO	4%	4%	3%	4%	2%

The feed rates for these 5 experiments were varied in a wide range from 0.05 to 0.9 mol/h. Despite the low reaction temperature of 220ºC, the methanol conversion was higher than 90% at the low flow rates whereas it dropped to 30% for the highest flow rate. The methanol conversion is calculated by assuming the SR reaction is the only reaction to take place. From the stoichiometry of SR reaction, 1 mol of methanol and 1 mol of water will generate 1 mol CO_2 and 3 moles H_2, or 4 moles product gas in total. The moles of methanol reacted to products per unit time were thus determined by dividing the measured gas product flow rate (converted from volumetric flow to molar flow) by 4. As the feed was injected in the reformer by syringe pump with controlled liquid flow rate, the conversion of methanol was calculated by dividing the methanol converted per unit time by the methanol molar feed rate. The product gas composition remained about the same regardless of the methanol conversion. It may be noted that the molar ratio of H_2 to CO_2 is higher than the stoichiometric ratio of the steam reforming reaction

(equation 1-3). It is speculated that this discrepancy may be associated with the fact that the product gas analyses were done off-line in a batch-wise manner using a limited amount of sample.

If the efficiency of a PEMFC is assumed to be 50%, hydrogen supply at a rate of 0.252 mol/h is required for 10W power generation. This is equivalent to the feed rate of 0.168 mol/h for the reactants that is an equimolar mixture of methanol and water. Thus, for when repeating the steam reforming experiments, the reactant feed rate was varied from 0.074 to about 0.61 mol/h, as this covered the range of about 0.5 to 4 times the flow rate that is needed to produce hydrogen for 10W power generation. The new results which were done online in a continuous manner with more duplicated compositional analysis measurements showed good agreement with the reaction stoichiometry of the steam reforming reaction. For each feed rate, 3 or more samples were measured by GC to get an average composition. The standard deviations were also calculated for each data point and added to Table 3-2.

Table 3-2 Product gas composition as a function of feed rate at steam reforming conditions (reaction temperature: 220ºC, Water to methanol molar ratio=1:1, Catalyst-3 was used for measurements, which is a mixture of fresh and used catalyst from the second batch [Catalyst-2])

Feed rate (mol/hr)	0.074	0.146	0.244	0.366	0.488	0.610
Product gas flow rate (mol/hr)	0.13	0.20	0.28	0.30	0.30	0.30
Methanol conversion	86%	70%	56%	42%	31%	25%
H_2%	72.36	72.49	72.50	72.61	72.58	72.76
CO_2%	27.52	27.42	27.42	27.31	27.34	27.16
CO%	0.11	0.08	0.08	0.08	0.08	0.08

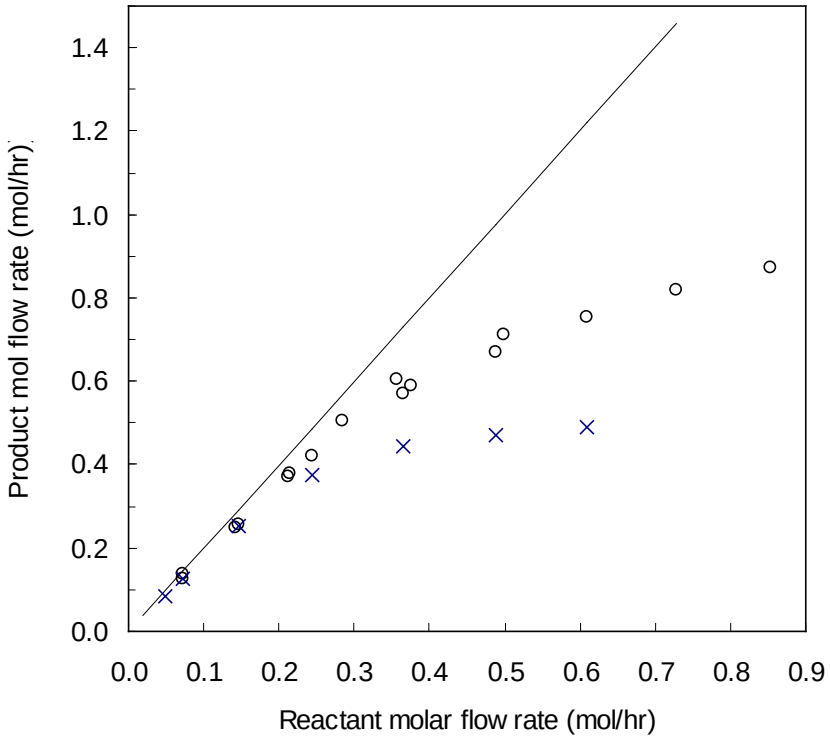

Figure 3-5 Product gas flow rate vs. feed flow rate (o: catalyst batch-1, ×: catalyst batch-2) at 220ºC. The solid line indicates the product molar flow rate expected

In Figure 3-5 the molar flow rate of the product gas is shown as a function of the feed flow rate for the two different catalyst batches. The two batches of catalyst are pretreated in the same way, i.e. activation by slow methanol/water feed rates in the absence of oxygen for 12 hours. Also shown in the figure is the line representing the ideal (or maximum) product gas flow rate that is equivalent to 100% conversion of methanol. When the feed flow rate is at 0.15 mol/h, the conversion of methanol is close to 100% and the behavior of Catalyst-2 is very close that of Catalyst-1. However, when the feed flow rate is doubled, to 0.3 mol/h, the conversions decrease to about 80% for Catalyst-1 and 62% for Catalyst-2. Further increase in the feed flow rate decreases the conversion even more making it lower than 50% even for catalyst-1 when the feed rate is about 0.9 mol/h. Although the catalysts were prepared following the same procedure, the

second batch of catalyst appeared to be of lower efficiency than the first batch and the prereduction of the catalysts might have reduced the differences between them.

3.3.1.2 Temperature effect

Low temperature operability is most desirable for a compact reformer for portable application, and the methanol conversion has been shown to be close to 100% for a targeted feed flow rate, i.e. the 0.168 mol/h feed rate of an equimolar mixture of methanol and water, which is needed for a 0.252 mol/h H_2 production rate required for power generation in a 10 W PEMFC, even at the lowest temperature recommended for the commercial catalyst. As the demand for hydrogen may increase, it is important to test both feed flow rates higher than the targeted feed flow rate and higher temperatures. As increasing the feed rate decreases the contact time, this results in a decrease in conversion (see Figure 3-5), to utilize more of the methanol, the temperature must be increased. Therefore, experiment were also conducted at 250ºC and compared to those conducted at 220ºC (see Table 3-3). The Catalyst-3 was used for this experiment as it was the latest batch and showed lower conversion than Catalyst-1 at 220ºC. The temperature thus expected to have a stronger influence on Catalyst-3 compared to Catalyst-1. The feed was also the equimolar mixture, and the feed flow rate was varied from 0.074 to 0.61 mol/h.

Table 3-3 Product gas composition as a function of feed rate at steam reforming conditions (reaction temperature: 250ºC, Water to methanol molar ratio=1:1)

Feed rate (mol/hr)	0.074	0.146	0.244	0.366	0.488	0.610
Product gas flow rate (mol/hr)	0.14	0.25	0.36	0.41	0.41	0.41
Methanol conversion	93%	87%	74%	56%	42%	34%
H_2%	72.94	72.21	72.54	71.85	72.56	72.48
CO_2%	26.72	27.63	27.27	28.04	27.35	27.44
CO%	0.34	0.16	0.19	0.11	0.09	0.08

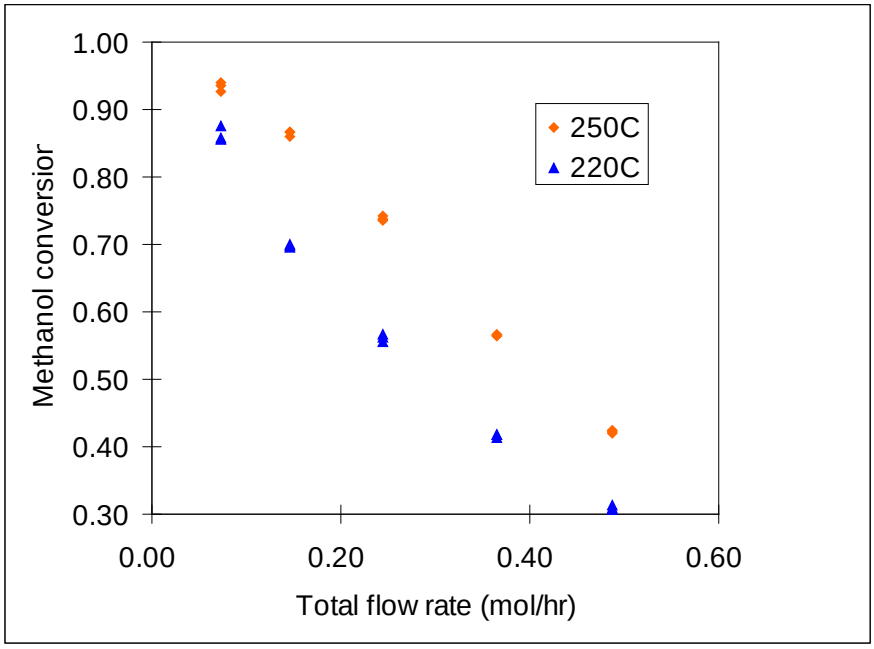

Figure 3-6 Conversion of methanol at various feed rates and reformer temperatures.

As Figure 3-6 indicates, the methanol conversion is slightly higher at a higher reaction temperature. At the feed flow rate of 0.146 mol/h, the conversion increases from 70% to 87% when the reaction temperature is increased from 220ºC to 250ºC, whereas it increases from 42%

to 56% at a feed rate of 0.366 mol/h. At 220ºC, the feed rate above which the conversion drops below 50% is about 0.3 mol/h, whereas it is 0.4 mol/h when the reaction temperature is 250ºC.

Consequently, if a higher H_2 flow rate is needed or if the catalyst deactivates slightly so that the desired H_2 production rate is not reached at 220ºC, it is possible to increase the temperature to increase methanol conversion and thus the H_2 yield.

3.3.1.3 Effect of methanol to water molar ratio of the feed

As increasing the water-to-methanol molar ratio of the feed has been shown to result in higher conversions, higher yields of hydrogen and higher selectivities to CO_2, the effect of varying water-to-methanol molar ratio was also investigated. The results are shown in Figures 3-7 and 3-8 as well as in Table 3-4. In these cases the product gas only consists of the non-condensable H_2, CO and CO_2.

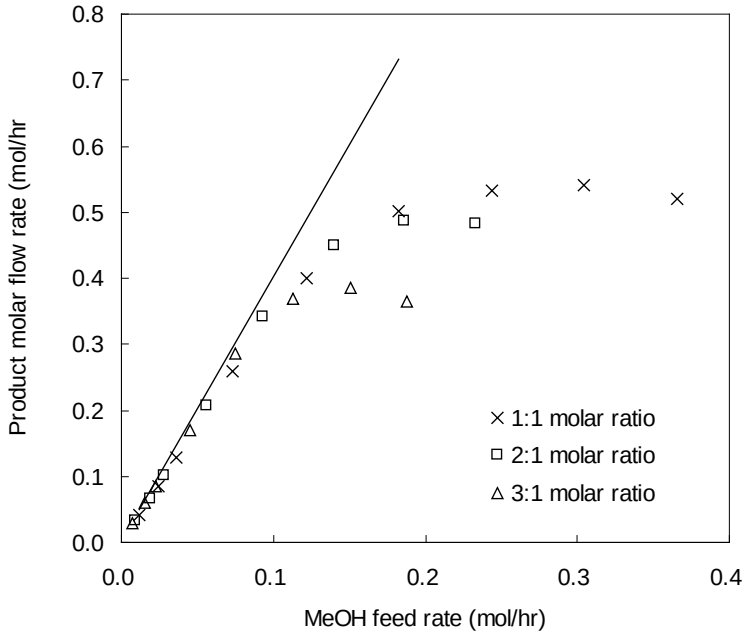

Figure 3-7 Influence of water-to-methanol molar ration on the product molar flow rate at various methanol feed rates (at 250ºC). The solid line represents the product gas flow rate at 100% conversion of MeOH, assuming only steam reforming and no reverse water-gas-shift or methanol decomposition reactions.

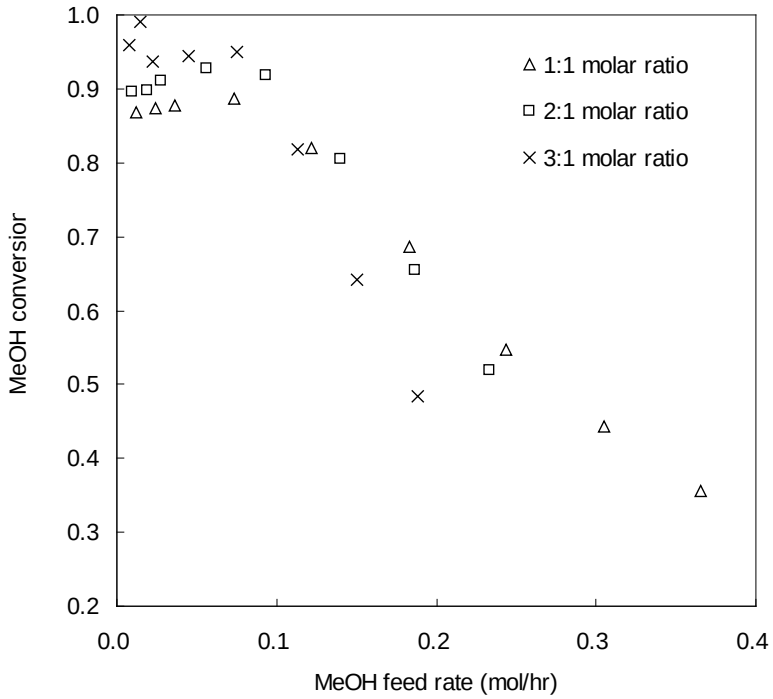

Figure 3-8 Influence of water-to-methanol molar ratio on methanol conversion at various methanol feed rates (at 250ºC).

Only at the lowest methanol feed rates, below 0.1 mol/h, does a higher water-to-methanol ratio appear to result in slightly higher product gas flow rate (Figure 3-7) and conversion of methanol (Figure 3-8), although the differences are not significant. In contrast, at a higher feed rate, the adverse effects of a larger water-to-methanol ratio was apparent in that both the product gas flow rate and the methanol conversion were lower than for the case of the equimolar mixture feed. At water-to-methanol molar ratio of 3 the decrease in conversion was rather significant in that it dropped below 50% at the methanol feed rate of about 0.2 mol/h. This is to be compared with a conversion of 65-69% at the same methanol feed rate, but water-to-methanol ratios of 1:1 and 2:1. This result may be associated with the fact that a higher water content in the feed at a high feed rate, would require much more energy for vaporization, and this could reduce the temperature in the reaction region. A reduced temperature, in turn, would reduce the methanol

conversion, potentially significantly which is the observed outcome. Having the ability to measure and control the temperature inside the catalyst bed would be very important to further probe the effects of varying water-to-methanol ratios and feed rates.

As the H_2:CO ratio is expected to vary with the H_2O-to-MeOH ratio, online GC measurement were performed to determine the product gas composition in these experiments (see Table 3-4). As is evident in the table, the hydrogen and CO_2 selectivities do not appear to change significantly with the water-to-methanol ratio. Only a slight decrease in CO concentration was observed, with increased water content in the feed. This indicated that the selectivity of the SR reaction is slightly improved over the methanol decomposition and the reverse water-gas-shift. However, the differences in CO concentrations are not significant in this case.

Table 3-4 Product gas composition at various water-to-methanol molar ratios (reformer temperature: 250ºC) with online GC measurements

MeOH feed rate (mol/hr)	0.12	0.12	0.12
Water feed rate (mol/hr)	0.12	0.24	0.36
Product gas flow rate (mol/hr)	0.40	0.41	0.39
Methanol conversion	82%	85%	81%
H_2%	72.54	72.21	72.04
CO_2%	27.27	27.66	27.85
CO%	0.19	0.13	0.12

3.3.2 Steam Reforming with Oxygen

3.3.2.1 Experimental results and theoretical predictions (19 channels of catalyst)

Experiments were carried out with catalyst in all 19 channels as a function of air flow rate. In this case the feed rates of methanol and water were fixed at 0.102 and 0.046 mol/h, respectively, while the air flow rate was varied between 0.102 to 0.335 mol/h. In the case of the low air flow rate (Experiment #1) there is not enough O_2 for autothermal reforming at this feed rate (i.e. to balance the heat released from the CPOX reaction and the heat needed in the reforming reaction). Assuming that the CPOX reaction is much faster than the reforming reaction, so that all the oxygen is depleted before the steam reforming reaction takes place, the theoretical values for the product flow rates and compositions can be calculated. These numbers are given in Table 3-5. In the theoretical estimate (predicted values) for the output gas flow rate it was assumed that only the steam reforming (SR) reaction and the catalytic partial oxidation (CPOX) reactions are taking place in the reformer. All other reactions are neglected. In each case, it is assumed that all the oxygen reacts, if there is a sufficient amount of methanol in the feed. In Experiment #1 methanol is in excess and the steam reforming is limited by the water, while methanol is the limiting reactant in Experiments #2 - #4. At the highest air flow rates, there is more O_2 added than needed for the partial oxidation reaction (Experiments #3 and #4), while in Experiment #2 only water is in excess.

For example, for Experiment #2 where the average air flow rate was 0.178 mol/h, the oxygen flow was 0.037 mol/h and it was assumed that $0.037 \times 2 = 0.074$ mol/h of methanol was consumed in the CPOX reaction (reaction 1-6). This leaves $0.102 - 0.074 = 0.028$ mol/h of methanol that can react in the steam reforming reaction. As there is 0.046 mol/h of water in the feed, this is sufficient to react all of the methanol in the SR reaction (this is not true in Experiment #1 as there is not enough water to react all the methanol in this case). The H_2 and

CO_2 product flow rates are then calculated according to the stoichiometries of the CPOX and SR reactions, i.e. one mol of methanol gives one mol of CO_2 and two moles of H_2 in the CPOX reaction and one mol of CO_2 plus three moles of H_2 in the SR reaction. All the details of the predicted values for each air flow rate are listed in Table 3-5.

Table 3-5 Theoretical calculation of gas flow rates and compositions as well as maximum conversions

Experiment series #	1	2	3	4
O_2 feed rate (mol/hr)	0.021	0.037	0.055	0.070
N_2 feed rate (mol/hr)	0.081	0.141	0.206	0.265
CH_3OH feed rate (mol/hr)	0.102	0.102	0.102	0.102
Water feed rate (mol/hr)	0.046	0.046	0.046	0.046
CH_3OH consumed by CPOX (mol/hr)	0.042	0.074	0.102	0.102
Limiting reactant [a]	Water	MeOH SR	MeOH PO	MeOH PO
CH_3OH consumed by SR (mol/hr)	0.046	0.028	0	0
H_2 generated by CPOX (mol/hr)	0.084	0.148	0.204	0.204
H_2 generated by SR (mol/hr)	0.138	0.084	0	0
CO_2 generated by CPOX (mol/hr)	0.042	0.074	0.102	0.102
CO_2 generated by SR (mol/hr)	0.046	0.028	0	0
Total product gas rate (mol/hr)	0.391	0.475	0.516	0.590
Theoretical CH_3OH conversion	86.3%	100%	100%	100%
Theoretical water conversion	100%	61%	0%	0%
Theoretical H_2 vol.% (N_2 free)	71.6%	69.5%	66.7%	66.7%
Theoretical CO_2 vol.% (N_2 free)	28.4%	30.5%	33.3%	33.3%

[a] MeOH SR: there is not enough methanol for the steam reforming reaction. MeOH PO: there is not enough methnol for the partial oxidation reaction.

The measured product gas flow rates and compositions for these experiments are given in Table 3-6. As can be seen in the table, the trend in the measured product gas flow rate and H_2:CO_2 ratio follows the predicted values, i.e. the product flow rate is increased, while the H_2:CO_2 ratio decreases with an increasing air flow rate.

Table 3-6 Product gas flow rate as a function of air flow rate at feed rates of 0.102 mol/h of methanol and 0.046 mol/h of water(with product gas composition from gas chromotograph) at T = 250ºC.

Exp.	Pressure	Feed	Product Flow Rates			Nitrogen-free product gas composition (%)			Exp.	Theo*
series #	at 3 psi	Air (mol/ h)	(ml/min)	(mol/h)	Theo. (mol/h) *	CO	CO_2	H_2	H_2/ CO_2	H_2/ CO_2
1	20.8	0.102	172	0.426	0.391	0.39	28.8	70.4	2.44	2.52
2	24.1	0.178	196	0.488	0.475	0.36	29.8	69.9	2.35	2.28
3	27.6	0.261	211	0.524	0.516	0.33	31.6	68.3	2.16	2
4	30.8	0.335	226	0.560	0.590	0.24	33.1	66.7	2.02	2

* Theoretical predition (see Table 3-5).

It should be noted the pressure at location 3 (i.e., P_3) was higher than 30 psi for the Experiment #4 in Table 3-5. These were for the cases where the position of the rotameter float was at 5. Because the air flow rate was relatively high for these cases, the pressure at location 1 (i.e., P_1) had to be raised to about 33 psi, and P_3 be greater than 30 psi unlike all other cases. Otherwise, the float poison 5 could not be obtained.

The measured gas compositions are also reasonably close to the predicted ones (Tables 3-5 and 3-6). Since only the CPOX and the SR reactions are considered in the calculations, the

predicted results do not contain any CO product. This appears to be a reasonable assumption as the measured CO concentration is less than 1% for all cases. This indicates that the contributions from the reverse water-gas-shift and methanol decomposition reactions are small under these conditions. As the reverse WGS and the MD reactions would reduce the H_2:CO_2 ratio, it is not surprising that the H_2:CO_2 ratio is lower than the predicted one assuming only CPOX and SR in Experiment #1. The fact that the measured ratio is higher than the predicted in the other cases (Experiments #2-#4) may suggest that the SR reaction does in fact compete with the CPOX reaction under certain conditions. In other words, more methanol is reacted in the steam reforming compared to the assumed amount based on the O_2 flow rate and the CPOX reaction (i.e. the values assumed in Table 3-5).

Although not very significant, the CO concentration appears to decrease slightly with increasing air flow rate. The higher oxygen concentration might have created an environment where oxidation of CO to CO_2 was more favorable thus decreasing the CO concentration. Despite the fact that the concentration of carbon monoxide is low, it is high enough to act as a poison to the catalyst in a PEMFC. Thus, installation of a gas cleaning unit will be necessary to remove CO prior to feeding the product gas to a PEMFC.

The data given in Table 3-5 and 3-6 combined together clearly indicated that the catalyst performance was sufficient to achieve near 100% conversion of methanol producing hydrogen at the rate between 0.2 and 0.23 mol/h. This production rate of hydrogen is slightly lower than the target value of 0.252 mol/h for a 10 W PEMFC operating at 50% efficiency. The lower rate was due to oxygen concentrations higher than needed for autothermal reforming, which resulted in more methanol being consumed by the CPOX reaction and less in the SR reforming reaction. These results indicate that the CPOX reaction does take place before the SR reaction under these

conditions, although perhaps not to the point where all the oxygen is consumed when oxygen is in excess. However, since the calculations on the feed rates on methanol and water were based on the autothermal case (where the heat generated by the CPOX reaction equals the heat needed in the SR reaction), the lower contribution from the SR reaction resulted in a lower H_2:CO_2 ratio and thus a lower H_2 flow rate than the targeted one.

As the liquid water flow rate in to the system is so small (0.83 ml/h), quantifying the water conversion by measuring the amount collected in the cold trap was not attempted in these cases. The same is true for the liquid methanol flow rate. It is therefore difficult to accurately determine the methanol conversion, as it is not possible to determine the fraction of methanol reacted in the steam reforming reaction versus that reacted in the partial oxidation reaction.

In order to increase the hydrogen production rate, the reactant feed rate or the temperature has to be increased. As the reaction does not appear to be conversion limited, higher feed rate experiments were also conducted for which the methanol and the water feed rates were 0.145 and 0.066 mol/h, respectively. These feed rates represent about 43% higher rates than the previous cases.

The results from the theoretical predictions are presented in Table 3-7. The numbers have been determined in the same way as in Table 3-5. As the methanol and water feed ratios are higher in these experiments while the air rates are the same, oxygen is never in excess (i.e. the partial oxidation reaction is never methanol limited). However, Experiment #2 in Table 3-7 is near autothermal reaction condition (heat released from the CPOX reaction balances the heat needed in the reforming reaction), in which >99% of reactants are consumed in this case. Therefore, assuming that all of the oxygen reacts, Experiments #1 and #2 have excess methanol and are limited by the water concentration, while in Experiments #3 and #4 the steam reforming

reaction is limited by methanol. Even though the maximum methanol conversion would be 78% in Experiment #1, the total combined hydrogen generation rate by the CPOX and SR reactions would be 0.29 mol/h, which is 14% higher than the target value of 0.252 mol/h for 10W PEMFC application. As the theoretical hydrogen production rate for full methanol conversion increases in the other Experiments, it should be practical to obtain this hydrogen production rate under these conditions. However, it is not advisable to run at the highest air feed rates as more of the hydrogen is produced via CPOX reaction, which has a lower H_2:CO_2 production ratio than the steam reforming reaction.

Table 3-7 Theoretical calculation of gas compositions and conversions (higher feed rate)

Experiment series #	1	2	3	4
O_2 feed rate (mol/hr)	0.0223	0.0389	0.057	0.071
N_2 feed rate(mol/hr)	0.0837	0.146	0.213	0.268
CH_3OH feed rate (mol/hr)	0.145	0.145	0.145	0.145
Water feed rate (mol/hr)	0.066	0.066	0.066	0.066
CH_3OH consumed by CPOX (mol/hr)	0.0466	0.0778	0.114	0.142
Limiting reactant	Water	Water	MeOH SR	MeOH SR
CH_3OH consumed by SR (mol/hr)	0.066	0.066	0.031	0.003
H_2 generated by CPOX (mol/hr)	0.0932	0.156	0.228	0.284
H_2 generated by SR (mol/hr)	0.198	0.198	0.093	0.009
CO_2 generated by CPOX(mol/hr)	0.0466	0.0778	0.114	0.142
CO_2 generated by SR (mol/hr)	0.066	0.066	0.031	0.003
Total product gas rate (mol/hr)	0.488	0.644	0.679	0.706
Theoretical CH_3OH conversion	77.7%	99.2%	100%	100%

Theoretical water conversion	100%	100%	47%	4.5%
Theoretical H_2 vol.% (N_2 free)	72.1%	71.1%	68.9%	66.9%
Theoretical CO_2 vol.% (N_2 free)	27.9%	28.9%	31.1%	33.1%

The measured data for these conditions are presented in Table 3-8. As the liquid feed rate was higher compared to the previous cases described in Table 3-5 and 3-6, the pressure at location 1 (i.e., P_1) was set at 35 psi, and P_2 was between 33 and 34 psi depending on the air feed rate.

Table 3-8 Product gas flow rate as a function of air flow rate at feed rates of 0.145 mol/h of methanol and 0.066 mol/h of water (with product gas composition from gas chromotograph) at T = 250ºC.

Exp.	Pressure	Feed	Product Flow Rates			Nitrogen-free product gas composition (%)			Exp.	Theo*
Series No.	at 3 (psi)	Air (mol/h)	(ml/min)	(mol/h)	Theo. (mol/h)*	CO	CO_2	H_2	H_2/CO_2	H_2/CO_2
1	23.0	0.106	218	0.542	0.482	0.66	26.83	72.51	2.7	2.58
2	26.6	0.185	255	0.634	0.644	0.43	28.58	70.98	2.48	2.46
3	29.8	0.270	276	0.684	0.680	0.36	30.28	69.36	2.29	2.22
4	33.5	0.339	288	0.716	0.704	0.36	31.11	68.54	2.20	2.02

* Theoretical predition (see Table 3-7).

As for the results at the lower feed rates, the measured product gas flow rate is in several cases slightly higher than the calculated values also for the higher feed rates. The largest deviation between the measured and the predicted values is at the lowest air flow rate (0.106 mol/h). This suggests that the assumptions made in calculating the product flow rates (Table 3-7) are not completely accurate. As the reaction in Experiment #1 is limited by water, and methanol

is in excess, it is possible that the methanol decomposition reaction contributes to the overall reaction in this case. This is supported by the higher CO concentration in the product compared to the other experiments at this feed flow rate. The agreement between the predicted and the measured production flow rates in the other experiments, suggest that the assumptions made in calculating the data in Table 3-7 are reasonable in those cases. The results indicate that the reformer can be used to produce sufficient hydrogen to run a 10 W fuel cell and the amount of catalyst in the reformer is sufficient to obtain 100% conversion of the methanol.

The measured H_2-to-CO_2 ratios for the experiments are also close to the predicted ones. In all cases the measured H_2-to-CO_2 ratio is slightly higher than the predicted one. A contribution from the methanol decomposition reaction can explain a higher H_2-to-CO_2 ratio as this reaction produces H_2 and CO and not CO_2. In Experiment #4, the higher H_2-to-CO_2 ratio and gas production rate compared to the predicted ones, are likely due also to a larger contribution from the steam reforming reaction and a lower than predicted CPOX reaction. In general the H_2 to CO_2 ratio is between 2 to 3, which is in agreement with the stoichiometries of SR (3:1) and CPOX (2:1 H_2:CO_2) reactions. The theoretical H_2 to CO_2 ratio for SR reaction is 3 and the ratio is 2 for CPOX reaction. In both Tables 3-7 and 3-8, the H_2 to CO_2 ratio is decreasing gradually as the air feed rate increases, which indicates an increasing contribution from the CPOX reaction, as expected from the higher O_2 concentrations.

3.3.2.2 Catalyst characterization

After completing the series of experiments on the steam reforming reaction with various amounts of oxygen present, it was observed that the catalyst in the different channels exhibited different colors. In fact, the catalysts particles in Channels 11-19 are lighter in color than the catalyst particles in Channels 20-29. This indicates a difference in the surface state of copper

between these catalysts. As the catalyst particles in Channels 20-29 do have a red tint, this could indicate some presence of Cu metal, i.e. reduced catalyst. This would be expected after exposure to reductive conditions, such as the steam reforming reaction. The presence of CuO was confirmed with XPS on the catalyst particles in Channel 11. This appears to indicate that the CPOX reaction indeed does take place in Channels 11-19, while the SR reaction occurs in the later half of the catalyst filled channels.

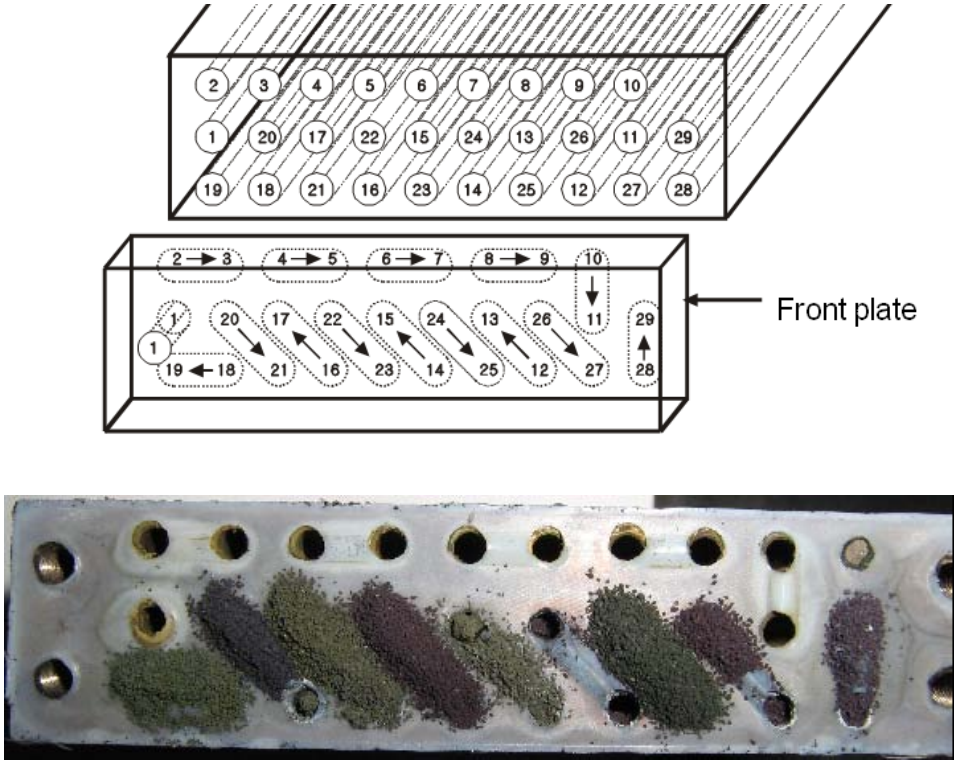

Figure 3-9 Catalysts in reformer channels after experiments

3.3.2.3 Experimental results and theoretical predictions (5 channels of catalyst)

As the kinetics of the commercial catalyst used in the reformer is not evaluated, it is not known if the CPOX reaction is as fast as the kinetics from Lin et al. (2007) suggests or if it significantly slower. Also, the results presented above does not reveal if the amount of catalyst

used in the reformer is more than enough to complete the reactions (i.e. the amount of catalyst is excessive). If the reaction can be completed in less channel length, the reformer volume/dimension can be smaller and more compact, which is in favor of the "compact" reformer target.

Table 3-9 Theoretical calculation of gas compositions and conversions (various feed rates)

Experiment series #	1	2	3	4	5	6	7	8
O_2 feed rate (mol/hr)	0.0155	0.0263	0.0370	0.0641	0.0162	0.0277	0.0401	0.0651
N_2 feed rate (mol/hr)	0.0585	0.0988	0.1390	0.2410	0.0608	0.1043	0.1509	0.2449
CH_4O feed rate (mol/hr)	0.102	0.102	0.102	0.102	0.145	0.145	0.145	0.145
Water feed rate (mol/hr)	0.046	0.046	0.046	0.046	0.066	0.066	0.066	0.066
CH_4O consumed by CPOX (mol/h)	0.031	0.053	0.074	0.102	0.032	0.055	0.080	0.130
Limiting reactant	Water	Water	MeOH SR	MeOH PO	Water SR	Water SR	Auto-thermal	MeOH SR
CH_4O consumed by SR (mol/hr)	0.046	0.046	0.028	0	0.066	0.066	0.066	0.0148
H_2 generated by CPOX (mol/hr)	0.062	0.105	0.148	0.204	0.065	0.111	0.160	0.260
H_2 generated by SR (mol/hr)	0.138	0.138	0.084	0.000	0.198	0.198	0.198	0.044
CO_2 generated by CPOX (mol/hr)	0.031	0.053	0.074	0.102	0.032	0.055	0.080	0.130
CO_2 generated by SR (mol/hr)	0.046	0.046	0.028	0	0.066	0.066	0.066	0.0148
Total product gas rate (mol/hr)	0.336	0.441	0.473	0.560	0.422	0.534	0.654	0.695
Theoretical CH_4O conversion%	75.57	96.57	100	100	67.82	83.75	100	100
Theoretical water conversion%	100	100	61	0	100	100	100	22
Theoretical H_2 vol.% (N_2 free)	72.20	71.16	69.47	66.67	72.76	71.78	71.03	67.76
Theoretical CO_2 vol.% (N_2 free)	27.80	28.84	30.53	33.33	27.24	28.22	28.97	32.24

Experiments were therefore performed with the reformer only filled with 5 channels of catalyst and the rest of the reformer channels left empty. The experiments are similar to the experiments with all 19 channels filled with catalyst. As in the previous section, it is assumed that the CPOX occurs before the SR reaction and the calculated product flow rates and compositions based on the feed rates of each component is given in Table 3-9.

For comparison and easier evaluation of the contribution from the steam reforming reaction, the calculations were repeated for the case where only the CPOX reaction takes place. In this case it is assumed that the CPOX reaction goes to completion in the first five channels, but no steam reforming will take place. The results are presented in Table 3-10.

Table 3-10 Theoretical calculation of gas compositions and conversions (various feed rates for CPOX rxn only)

Experiment series #	1	2	3	4	5	6	7	8
O_2 feed rate (mol/hr)	0.0155	0.0263	0.0370	0.0641	0.0162	0.0277	0.0401	0.0651
N_2 feed rate (mol/hr)	0.0585	0.0988	0.1390	0.2410	0.0608	0.1043	0.1509	0.2449
CH_3OH feed rate (mol/hr)	0.102	0.102	0.102	0.102	0.145	0.145	0.145	0.145
CH_3OH consumpt. rate (mol/hr)	0.031	0.053	0.074	0.102	0.032	0.055	0.080	0.130
H_2 generation rate (mol/hr)	0.062	0.106	0.148	0.204	0.065	0.111	0.160	0.260
CO_2 generation rate (mol/hr)	0.031	0.053	0.074	0.102	0.032	0.055	0.080	0.130
Total product gas rate (mol/hr)	0.152	0.258	0.361	0.560	0.158	0.270	0.391	0.635
Theoretical CH_3OH conversion	30.39%	51.96%	72.55%	100%	22.07%	37.93%	55.17%	89.66%
Theoretical H2 vol.% (N2 free)	66.67%	66.67%	66.67%	66.67%	66.67%	66.67%	66.67%	66.67%
Theoretical CO2 vol.% (N2 free)	33.33%	33.33%	33.33%	33.33%	33.33%	33.33%	33.33%	33.33%

Total product gas rate (mol/hr) is the summation of H_2 , CO_2 with Nitrogen generation rate.

The actual measured product flow rates and product compositions are presented in Table 3-11. By comparing the data of the measured product gas flow rates to those presented in Table 3-9, it is evident that the measured results are lower in all cases comparing the theoretical estimations assuming complete CPOX and SR reactions. It is also notable that the measured H_2/CO_2 ratios are lower than predicted ratios in all cases (except in Experiment #8, where measured and predicted values are similar, see Table 3-11). As only 5 of the 19 channels are filled with catalyst, it is expected that both the CPOX and the SR reactions are not completed.

Table 3-11 Product gas flow rate as a function of air flow rate at two feed rates of methanol and water (0.102 and 0.046 mol/h, as well as 0.145 and 0.066 mol/h) and product gas composition from gas chromotography.

Exp.	Feed	Product Flow Rates			Product gas composition (%)			Exp.	Theo.*
Series No.	Air (mol/h)	(ml/min)	mol/h	Theo. (mol/h)*	CO	CO_2	H_2	H_2/ CO_2	H_2/ CO_2
Feed flow rates: 0.102 mol/h methanol and 0.046 mol/h water.									
1	0.074	87.3	0.217	0.336	0.10	27.94	71.95	2.58	2.60
2	0.125	10	0.272	0.441	0.18	29.42	70.40	2.39	2.47
3	0.176	129	0.320	0.473	0.18	32.05	67.77	2.12	2.28
4	0.305	156	0.388	0.560	0.21	33.53	66.25	1.98	2.00
Feed flow rates: 0.145 mol/h methanol and 0.066 mol/h water.									
5	0.077	87.6	0.218	0.422	0.15	28.40	71.44	2.52	2.67
6	0.132	110	0.274	0.534	0.23	30.08	69.69	2.32	2.54
7	0.191	158	0.393	0.654	0.30	31.95	67.75	2.12	2.45
8	0.310	176	0.437	0.695	0.21	32.12	67.68	2.11	2.10

* Theoretical predition (see Table 3-9).

Therefore, it is important to also compare the measured results to the case of CPOX only, since this reaction is assumed to be the faster one. It can be seen that the measured product gas flow rates are higher than those predicted from the CPOX reaction at low air flow rates, but lower at high air flow rates. Table 3-11 reveal that the H_2 concentrations for the low air flow rates are higher than those expected for CPOX reaction only (i.e. they are above 66.67%). This indicates that at the lower air flow rates the contribution from the steam reforming reaction is significant. In contrast, at high air flow rates the measured product gas flow rates and compositions are very close to the ones predicted from the CPOX reaction. Therefore, it appears

that the partial oxidation reaction is indeed fast and that no steam reforming takes place as long as there is oxygen present in the reactor. At least the steam reforming reaction will not be initiated as long as the oxygen partial pressure is above a certain level. This level was not quantified in the study, but oxygen at concentration levels below 1% (~0.1-0.4%) could be detected in all reactions involving air.

Comparing the results between the 5 and the 19 channels of catalyst (Tables 3-6, 3-8 and 3-11), it is evident that 5 channels of catalyst are not sufficient to complete the steam reforming reaction under these conditions. This is the reason that the product gas flow rates and the H_2/CO_2 ratios are lower in the 5 channel catalyst experiment compared to the 19 channel catalyst experiment. As more methanol is converted in the steam reforming reaction for the case of more catalyst channels, the product gas flow rate and the H_2/CO_2 ratio increase. Considering that a significant amount of reforming occurs at low flow rates, it is likely that 19 channels are not needed for 100% conversion (or to reach the limiting conversion).

3.4 Heat Transfer Aspects of the Reformer

Self-sustainability is one of the important features of the reformer in that the heat produced by the exothermic CPOX reaction is sufficient enough to maintain the endothermic steam reforming reaction. Due to incomplete insulation, however, some heat is lost to the environment and energy from an external source has to be provided unless the CPOX reaction can fully compensate for the heat loss to the environment. As it was difficult to identify the exact condition in which the heat produced by the CPOX counter balances the heat required by the steam reforming reaction and the heat loss to the environment, the following experiments were conducted to assess the heat transfer characteristics of the reformer:

- With the methanol and the water feed rates fixed at 0.145 and 0.066 mol/h respectively, the

air feed rate was varied at three levels; 0.0 (i.e., no oxygen supply), 0.186 and 0.339 mol/h.

- Temperature of the heat controller was set at 250°C, and experiment was run until steady state was reached. Under the steady state condition, the heater mounted on the reformer would be turned on and off intermittently due to the heat loss to the environment.
- Once the steady state is reached under each condition, experiment was run further for 10 to 15 more minutes. Then, the electrical supply to the heater was cut off and the temporal variation of the reformer temperature was monitored.

Due to incomplete insulation of the reformer, the heat loss to the outside environment would result in gradual decrease of the temperature. In the absence of oxygen supply, only the steam reforming reaction, that is endothermic, would occur and the temperature decrease would be faster than the cases with oxygen supply. Since the steam reforming reaction is endothermic, the temperature decay is expected to be even faster than the reference case in which no chemical reaction would occur because the catalyst was replaced with the glass beads. In Figure 3-10, the results for the temperature variation are given.

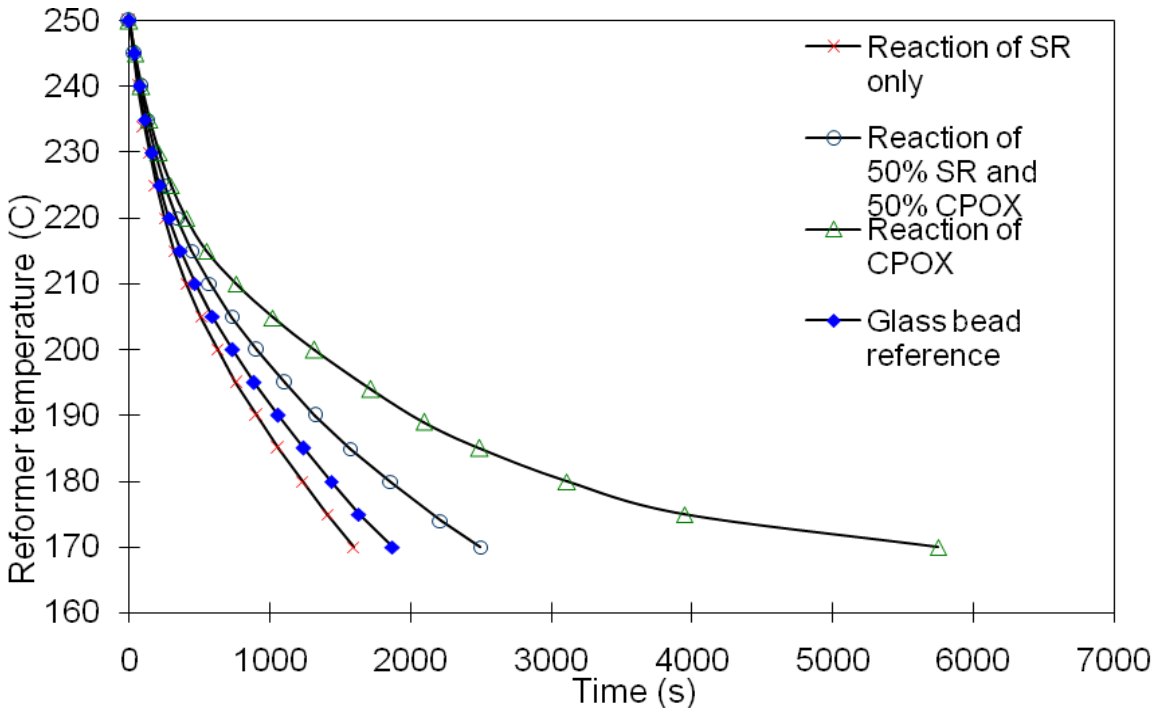

Figure 3-10 Temporal variation of the reformer temperature when the electrical power supply is cut off

In the absence of oxygen supply, it took 1592 seconds (26.5 minutes) for the temperature to drop from 250°C to 170°C whereas it took 2495 sec (41.6 min) and 5752 sec (95.9 min) when the air feed rate was 0.186 and 0.339 mol/h, respectively. Air feed rate of 0.186 mol/h is equivalent to the case of experiment #2 in Table 3-8, in which 54% of methanol is expected to be consumed by the CPOX reaction and the balance by the SR reaction. When the air feed rate is 0.339 mol/h (equivalent to experiment #4 in Table 3-8), on the other hand, most methanol is expected to be consumed by the CPOX reaction. Thus, the time for the temperature decrease would take longer with the increasing air feed rate in accordance with the experimental observation. The reference case is also shown in the figure in which the catalyst was replaced with the inactive glass bead. The curve for the reference case is expected to be located above the

case for the steam reforming reaction only because the SR is endothermic inducing faster temperature decay. The experimental results are in fact in accordance with the expectation.

It should be pointed out that temperature decrease was realized even when the methanol was consumed mostly by the CPOX reaction (i.e., when the air feed rate was 0.339 mol/h) although it took longer than 1.5 hours for the temperature to drop from 250°C to 170°C. It is mainly due to the fact that the rate of heat loss to the environment is still larger than the rate of heat generation by the CPOX reaction although the reformer is insulated using fiber glass.

Heat Balance: The unsteady heat balance for the reformer is given as

$$\dot{E} = \frac{dE}{dt} = \dot{E}_{in} - \dot{E}_{out} + \dot{E}_{g} \tag{3-6}$$

Here $\dot{E}$ is the rate of change of energy within the reformer; $\dot{E}_{in}$ and $\dot{E}_{out}$ are the input and output rates of energy to the system (i.e., reformer) accompanied by the materials going in and out of the reformer. $\dot{E}_{g}$ is the net rate of heat generation that accounts for the heat generated by the chemical reactions as well as the heat loss to the environment. Thus, equation (3-6) is given as

$$\dot{E} = \frac{dE}{dt} = \sum_{i} \dot{m}_i \hat{H}_i - \sum_{j} \dot{m}_j \hat{H}_j + \dot{E}_{gen} + \dot{E}_{loss} \tag{3-7}$$

Here $\dot{m}_k$ and $\hat{H}_k$ are the mass flow rate and the specific enthalpy of species k. The subscript i and j are the chemical species in the input and output streams, respectively.

Because the input materials (i.e., methanol, water, oxygen and nitrogen) and their flow rates are specified, $\dot{m}_i$ and $\hat{H}_i$ are known. However, the flow rates of the materials in the output stream, $\dot{m}_j$, are not known unless the conversion is known. For the estimation of the transient

heat transfer characteristics, we considered the case in which the heat generated by the CPOX reaction is balanced with the heat consumed by the steam reforming reaction. That is

$$\sum_i \dot{m}_i \hat{H}_i - \sum_j \dot{m}_j \hat{H}_j + \dot{E}_{gen} = 0 \tag{3-8}$$

Thus, $$\frac{dE}{dt} = \dot{E}_{loss} \tag{3-9}$$

It represents the case in which the transient temperature of the reformer is strictly determined by the heat loss to the environment. Equation (3-9) is valid only when the conversion is 100% for the given flow rates of ideal mixture described in section 3.1.2. As long as the reformer temperature is above about 200°C, both CPOX and SR reactions will persist with complete conversion. However, if the reformer temperature becomes lower than about 200°C, the conversion will be less than 100% and equations (3-8) and (3-9) will become invalid.

The temperature of the reformer may depend on both position and time. However, the spatial variation of the temperature may be negligible because the thermal resistance within the reformer is much smaller than that for the outside environment including the insulation. The ratio of these heat resistances is represented by the following Biot number [93]

$$Bi = \frac{hL_c}{k} \tag{3-10}$$

Here k is the thermal conductivity of the material that constitutes the reformer (i.e., stainless steel), L_c is the characteristic length of the reformer and h is the overall heat transfer coefficient that accounts for the insulation as well as the air layer outside the insulation. That is,

$$\frac{1}{h} = \frac{1}{h_{air}} + \frac{t}{k_{insulation}} \tag{3-11}$$

where h_{air} is the convective heat transfer coefficient of the air layer, $k_{insulation}$ is the thermal conductivity of the insulation, and t is its thickness.

If the Biot number is smaller than about 0.1, it is generally accepted that the spatial variation of the temperature within the reformer is negligible and the so-called lumped capacitance method can be used for the thermal analysis in that only temporal variation of the reformer is considered for the transient heat transfer problem. For the present case, k for stainless steel is known to be 16.6 and 19.8 W/m-K at 400K and 600K, respectively [93], L_c is 0.9 cm for the reformer, h_{air} is about 10 W/m^2-K for natural convection [94], the insulation thickness t is 2 cm, and the thermal conductivity of the insulation material is between 0.06 W/m-K at 170°C and 0.08 W/m-K at 250°C [95]. Thus, h is calculated to be 2.9 W/m^2-K, and the Biot number is 1.6×10^{-3}. Because the Biot number is much smaller than 0.1, the lumped capacitance method can be used. Therefore, equation (3-9) is given as

$$\rho Vc\frac{dT}{dt} = -hA(T - T_\infty) \tag{3-12}$$

Here ρ, V, and c are the density, volume and the heat capacity of the reformer. A is the surface area of the reformer and h the overall heat transfer coefficient given in equation (3-11). T is the reformer temperature at time t and T_∞ is the temperature of the air far away from the reformer surface.

For constant values of ρ, V, c and h, equation (3-12) is integrated to be

$$\frac{T - T_\infty}{T_i - T_\infty} = \exp(-\frac{hA}{\rho Vc})t \tag{3-13}$$

where T_i is the initial temperature of the reformer at the time when the electrical heater is turned off. The heat capacity of stainless steel is known to be 0.528 J/mol-K at 170°C and 0.540 J/mol-K at 250°C [96].

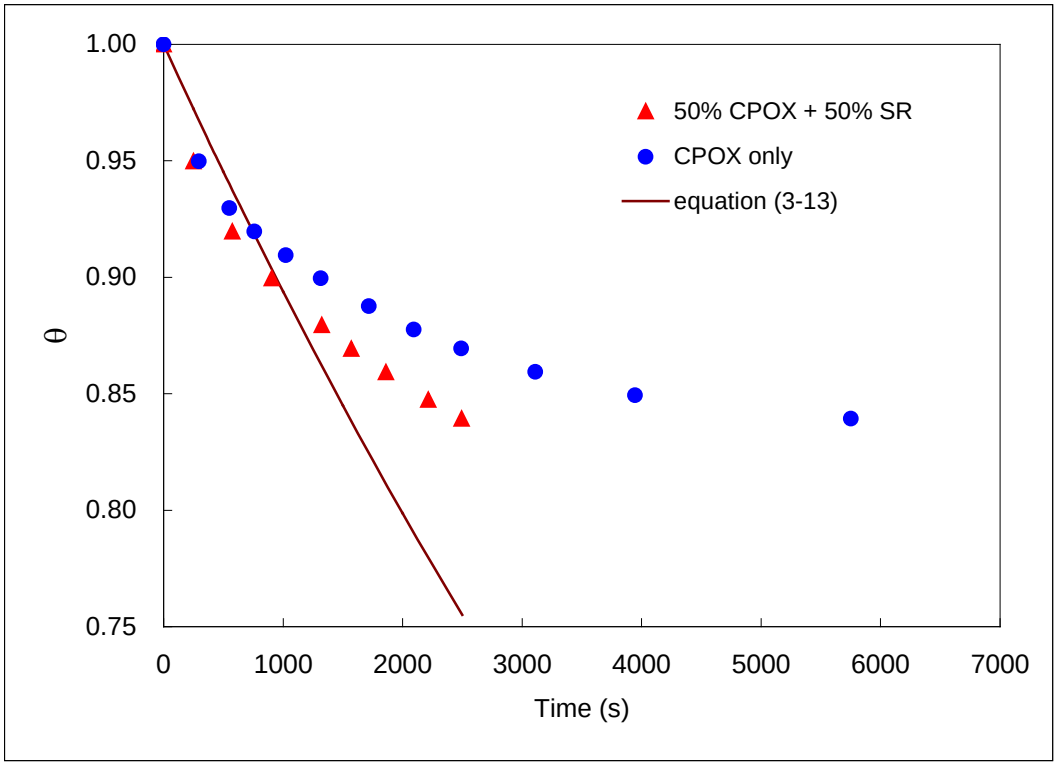

Figure 3-11 Temporal variation of $[(T-T_\infty)/(T_i-T_\infty)]$ when the electrical power supply is cut off

In Figure 3-11, the dimensionless temperature, $\theta = \frac{T - T_\infty}{T_i - T_\infty}$, for two different experimental conditions is given along with the prediction by equation (3-13). Because equation (3-13) is close to the ideal case for which equation (3-8) is valid, it is appropriate to compare this prediction with the case of 50% CPOX and 50% SR reaction. As it was pointed out previously, equation (3-13) will not be valid if the temperature is lower than about 200°C (i.e., $\theta < 0.78$) and it is plotted until θ decreases to about 0.78. It is apparent that the experimental observation does not match well with the prediction by equation (3-13). This discrepancy may be due to the fact that equation (3-13) includes numerous simplifying assumptions such as dimensional simplification as well as uncertainties associated with the values for heat transfer coefficient and

material properties. It seems that a full three-dimensional analysis has to be applied for better prediction of heat transfer characteristics of the reformer.

When the oxygen feed rate is high, methanol is totally consumed the CPOX reaction and the heat generation rate is maximum at about 5.3 W. According figure 3-10, the reformer temperature decreases even for this case indicating that the heat loss to the environment is greater than 5.3 W. According to equation (3-12), the instantaneous heat loss at t=0 is about 11 W, which in fact is much larger than 5.3W as expected. According to figure 3-11, the initial temperature decay (i.e., the slope of θ at t=0) of the experimental observation appears to be larger than predicted value by equation (3-12) indicating that the actual heat loss at t=0 is even larger than 11 W. This result indicates that proper insulation of the reformer is very important for self-sustainability and the current insulation is not sufficient. Nevertheless, all these results support that the prototype reformer is capable of meeting the preset requirements to produce enough hydrogen for 10W PEMFC application. It seems that its size probably can be reduced to make it even smaller. Smaller size would be also helpful for better insulation as the external surface area of the reformer would decrease. One aspect that could not be evaluated by the present study is longevity of the catalyst. For such evaluation, the reformer may have to be run continuously for months. In the present study, though, the same catalyst was used for numerous intermittent runs that lasted for tens of hours over several months period.

CHAPTER 4
CONCLUSIONS AND FUTURE WORK

A new design idea for a compact reformer for portable applications has been proposed. This reformer, in a sense, is a conventional tubular reactor type because it consists of a cylindrical channel packed with catalyst particles although some design features such as interlaced channel structure are rather unique. Flow simulation has been conducted to determine the dimension of the reformer that is appropriate for a PEMFC with the electrical energy production rate of 10 W. A prototype reformer has been built based on the simulation result and experiments have been conducted to assess the viability of the reformer using a commercial catalyst of $CuO/ZnO/Al_2O_3$ type and mixtures of methanol and water as the feed. In the absence of oxygen, methanol conversion higher than 80% could be obtained at a reaction temperature lower than 250˚C and at a moderately high pressure of about 2 atm. When oxygen was added to the system in the form of air, the catalytic partial oxidation (CPOX) reaction occurred along with the steam reforming (SR) reaction achieving complete conversion of methanol. It is likely that 19 channels of catalyst are not needed for 100% conversion (or to reach the limiting conversion), and the amount of catalyst may be reduced in fabricating the reformer.

The results of the present study support the viability of the new design idea in that the exothermic CPOX reaction occurs along with the endothermic SR reaction with efficient heat transfer characteristics. Other advantages of this reformer may include compactness, easy incorporation of the catalyst and efficient thermal management. Although the heat from the exothermic CPOX reaction can be used for the endothermic SR reaction eliminating the need for an external energy source for the reformer to function, an external energy source is still required for the startup operation. Furthermore, heat loss to the outside environment occurs due to incomplete insulation, and an external energy source may be necessary even during a steady state

operation unless the heat loss is also compensated by the exothermic reaction. As the heat loss to the environment is inevitable no matter how good the insulation may be, accurate quantification of the heat transfer characteristics will be essential for a proper design of the reformer. To better characterize the performance of the reformer, it will also be helpful if the temperatures inside the channels can be measured although it may be very difficult.

APPENDIX

HEAT OF REACTION AT THE OPERATING TEMPERATURE OF THE REFORMER

The heat of reaction at the operating temperature of the reformer (i.e., 250°C) is calculated here using the values of the standard heat of reaction and the thermodynamic properties of the materials involved.

CPOX Reaction

The heat of reaction at 25°C is given by:

CH_3OH (l, 25°C) + ½ O_2(g, 25°C) ↔ CO_2(g, 25°C) + $2H_2$(g, 25°C) (ΔH_0 = – 154.9 kJ/mol) (1-6)

where ΔH_0 is the standard heat of reaction.

CH_3OH(l, 25°C) + ½ O_2(g, 25°C) ↔ CO_2(g, 250°C) + $2H_2$(g, 250°C) (ΔH)

where ΔH is the heat of reaction at the operating temperature of the reformer, 250°C.

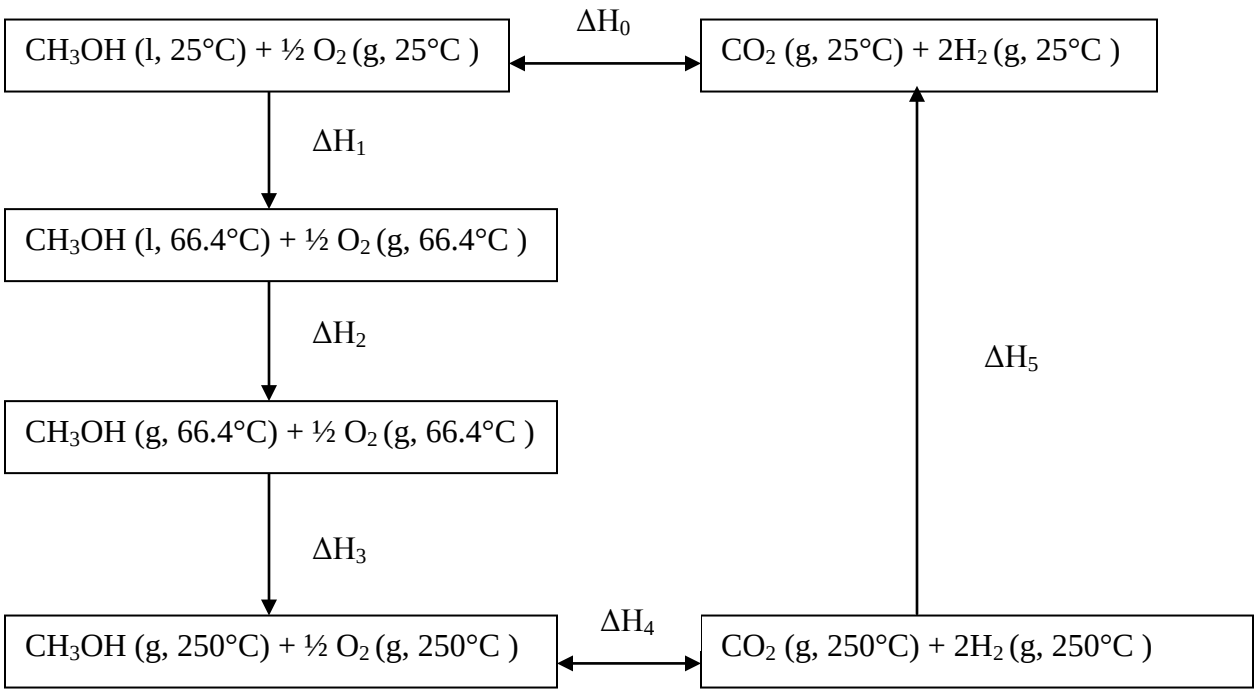

Since $\Delta H_0=\Delta H_1+\Delta H_2+\Delta H_3+\Delta H_4+\Delta H_5$, $\Delta H=\Delta H_1+\Delta H_2+\Delta H_3+\Delta H_4=\Delta H_0-\Delta H_5$. And ΔH_5 can be calculated using the heat capacities of carbon dioxide and hydrogen.

* Heat capacity of CO_2

Heat capacity (J/mol) At 25 °C (gas)	0.0372	kJ/mol/°C
Heat capacity (J/mol) At 250 °C (gas)	0.0467	kJ/mol/°C
heat from 25°C to 250°C	9.44	kJ/mol

ΔH from 25°C to 250°C may be calculated either using the average heat capacity or using the Cp(T) data. Here the average heat capacity is used and

ΔH = (0.0467+0.0372)/2*(250-25)=9.44 kJ/mol

* Heat capacity of H_2

Heat capacity (J/mol) at 25 °C (gas)	0.0288	kJ/mol/°C
Heat capacity (J/mol) at 250 °C (gas)	0.0288	kJ/mol/°C
heat from 25°C to 250°C	6.49	kJ/mol

Similarly ΔH for hydrogen is calculated to be 6.49 kJ/mol using the average heat capacity.

Therefore, the heat of reaction of the CPOX reaction at 250 °C is

$\Delta H=\Delta H_0-\Delta H_5$= -154.9- (-9.44-6.49*2) = -132.48 kJ/mol

Steam Reforming Reaction

CH_3OH (l, 25°C) + H_2O (l, 25°C) ↔ CO_2(g, 25°C) + $3H_2$(g, 25°C) ($\Delta H'_0$ = 130.9 kJ/mol) (1-3)

CH_3OH (l, 25°C) + H_2O (l, 25°C) ↔ CO_2 (g, 250°C) + $3H_2$(g, 250°C) ($\Delta H'$)

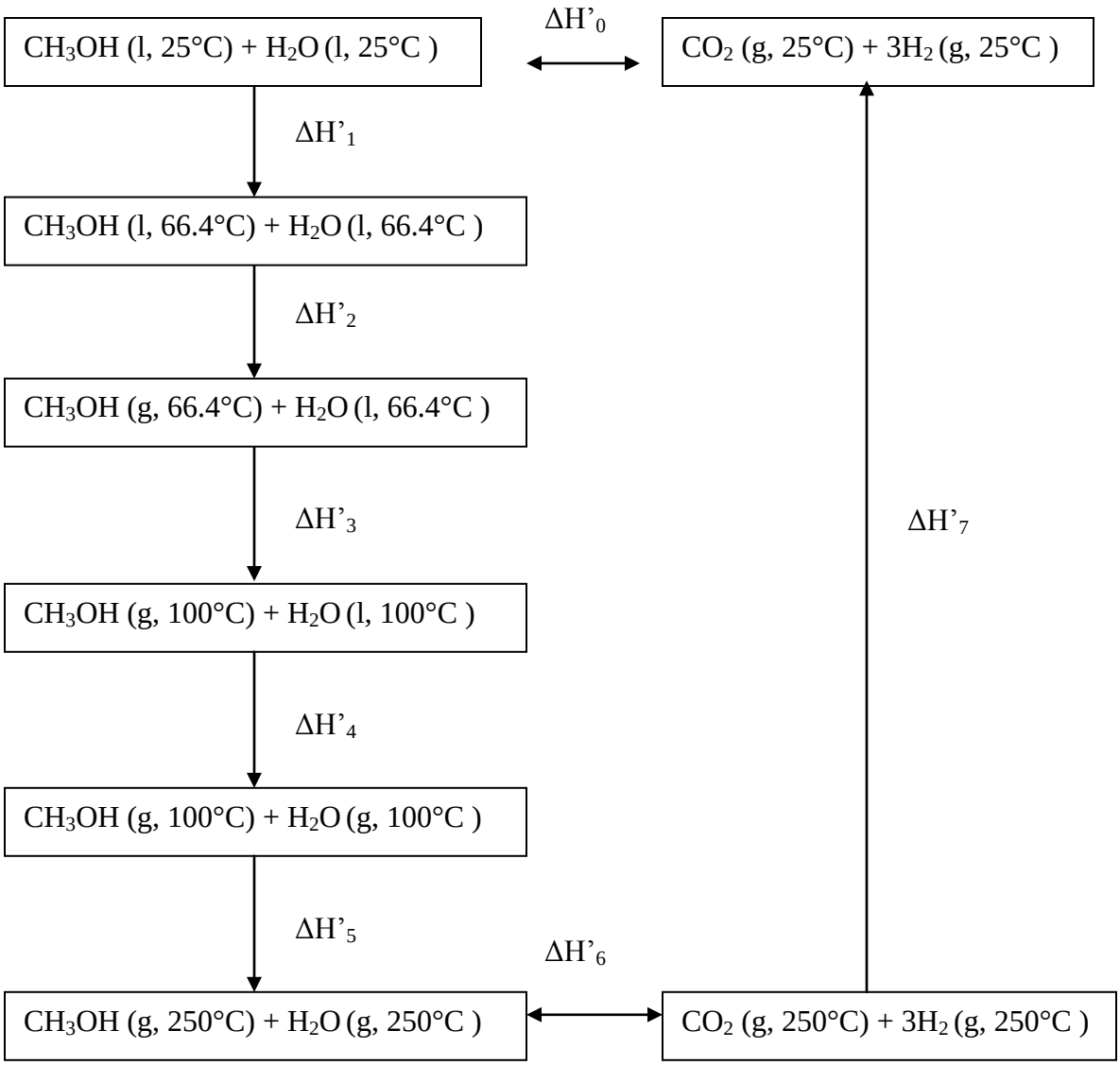

$\Delta H'_0=\Delta H'_1+\Delta H'_2+\Delta H'_3+\Delta H'_4+\Delta H'_5+\Delta H'_6+\Delta H'_7$

$\Delta H'=\Delta H'_1+\Delta H'_2+\Delta H'_3+\Delta H'_4+\Delta H'_5+\Delta H'_6=\Delta H'_0-\Delta H'_7$

$\Delta H'_7$ is again calculated using the heat capacity data. Thus,

$\Delta H'=\Delta H'_0-\Delta H'_7$=130.9- (-9.44-6.49*3) =159.8 kJ/mol

LIST OF REFERENCES

[1] M. Francis, Modeling: driving fuel cells, Materials Today 5(5) (2002) 34-39.

[2] C. Song, Fuel processing for low-temperature and high-temperature fuel cells Challenges, and opportunities for sustainable development in the 21st century, Catalysis Today 77 (2002) 17-49.

[3] L. Carrette, K.A. Friedrich, U. Stimming, Fuel cells - Fundamentals and applications Fuel Cell 1 (2001) 5-39.

[4] V. Mehta, J.S. Cooper, Review and analysis of PEMFC fuel cell design and manufacturing, Journal of Power Sources 114 (1) (2003) 32-53.

[5] J. St-Pierre, D.P. Wilkinson, Fuel Cells: a New, Efficient and Cleaner Power Source, AIChE Journal 47(7) (2001) 1482-1486.

[6] Fuel Cell Handbook, 7th edition, U.S. Dept. of Energy, Nov. 2004.

[7] K. Sopian, W.R.W. Daud, Challenges and future developments in proton exchange membrane fuel cells, Renewable Energy 31 (5) (2006) 719-727.

[8] S.M. Haile, Fuel cell materials and components, Acta Materialia 51 (19) (2003) 5981-6000.

[9] G.F. McLean, T. Niet, S. Prince-Richard, et al., An assessment of alkaline fuel cell technology, International Journal of Hydrogen Energy 27 (5) (2002) 507-526.

[10] F. Alcaide, P. Cabot, E. Brillas, Fuel cells for chemicals and energy cogeneration, Journal of Power Sources 153 (1) (2006) 47-60.

[11] E. Antolinia, J.R.C. Salgadob, E.R. Gonzaleza, The stability of Pt-M (M = first row transition metal) alloy catalysts and its effect on the activity in low temperature fuel cells. A literature review and tests on a Pt-Co catalyst, Journal of Power Sources 160 (2) (2006) 957-968.

[12] N. Sammes, R. Bove, K. Stahl, Phosphoric acid fuel cells: Fundamentals and applications, Current Opinion in Solid State and Materials Science 8 (5) (2004) 372-378.

[13] L.-J. Yu, G.-P. Ren, X.-M. Jiang, Experimental and analytical investigation of molten carbonate fuel cell stack, Energy Conversion and Management 49 (4) (2008) 873-879.

[14] T. Ishikawa, H. Yasue, Start-up, testing and operation of 1000 kW class MCFC power plant, Journal of Power Sources 86 (1-2) 2000. 145-150

[15] M. Bischoff, Molten carbonate fuel cells: A high temperature fuel cell on the edge to commercialization, Journal of Power Sources 160 (2) (2006) 842-845.

[16] P. Tomczyk, MCFC versus other fuel cells—Characteristics, technologies and prospects, Journal of Power Sources 160 (2) (2006) 858-862

[17] S. Campanari, Carbon dioxide separation from high temperature fuel cell power plants, Journal of Power Sources 112 (1) (2002) 273-289.

[18] S. Scaccia, S.Frangini, S. Dellepiane, Enhanced O_2 solubility by RE_2O_3 (RE = La, Gd) additions in molten carbonate electrolytes for MCFC, Journal of Molecular Liquids 138 (1-3) (2008), 107-112.

[19] M. Z. Hong, S. C. Bae, H. S. Lee, et al., A study of the Co-coated Ni cathode prepared by electroless deposition for MCFCs, Electrochimica Acta 48 (28) (2003) 4213-4221.

[20] S. P. S. Badwal**,** Stability of solid oxide fuel cell components, Solid State Ionics 143 (1) (2001) 39-46.

[21] N. Q. Minh, Solid oxide fuel cell technology—features and applications, Solid State Ionics 174 (1-4) (2004) 271-277.

[22] M. Yano, A. Tomita, M. Sano, Recent advances in single-chamber solid oxide fuel cells: A review, Solid State Ionics 177 (39-40) (2007) 3351-3359.

[23] J. W. Fergus, Oxide anode materials for solid oxide fuel cells, Solid State Ionics 177 (17-18) (2006) 1529-1541.

[24] M. Lyubovsky, S. Roychoudhury, Novel catalytic reactor for oxidative reforming of methanol, Applied Catalysis B: Environmental 54 (4) (2004) 203-215.

[25] J.-H. Wee, Applications of proton exchange membrane fuel cell systems, Renewable Sustainable Energy Reviews 11 (8) (2007) 1720-1738.

[26] H.A. Gasteiger, J.E. Panels, S.G. Yan. Dependence of PEM fuel cell performance on catalyst loading, Journal of Power Sources 127 (1-2) (2004) 162-171.

[27] S. Y. Hwang, H-I Joh, M.A. Scibioh, et al., Impact of cathode channel depth on performance of direct methanol fuel cells, Journal of Power Sources 183 (1) (2008) 226-231.

[28] E. Bostic, N. Sifer, C. Bolton, et al., The US army foreign comparative test fuel cell program, Journal of Power Sources 137 (1) (2004) 76-79.

[29] R. Dillon, S. Srinivasan, A.S. Aricò, et al., International activities in DMFC R&D: status of technologies and potential applications, Journal of Power Sources 127 (1-2) (2004) 112-126.

[30] V. Neburchilov, J. Martin, H. Wang, et al., A review of polymer electrolyte membranes for direct methanol fuel cells, Journal of Power Sources 169 (2) (2007) 221-238.

[31] J.R. Rostrup-Nielsen, Conversion of hydrocarbons and alcohols for fuel cells. Phys. Chem. Chem. Phys., 3 (2001) 283-288.

[32] J.O. Jensen, Q. Li, C. Pan, et al, High temperature PEMFC and the possible utilization of the excess heat for fuel processing. 32 (2007) 1567-1571.

[33] C.L.Yaws, Chemical properties handbook physical, thermodynamic, environmental, transport, safety, and health related properties for organic and inorganic chemicals. McGraw-Hill (1999)

[34] P.M. Biesheuvel, J.J.C. Geerlings, Thermodynamic analysis of direct internal reforming of methane and butane in proton and oxygen conducting fuel cells. Journal of Power Sources 185 (2008) 1162 – 1167.

[35] L. Zhou, Y. Guo, Q. Zhang, et al, A novel catalyst with plate-type anodic alumina supports, Ni/$NiAl_2O_4$/γ-Al_2O_3/alloy, for steam reforming of methane. Applied Catalysis A: General 347 (2008) 200-207.

[36] Y. Chen, Y. Wang, H. Xu, et al, Hydrogen production capacity of membrane reformer for methane steam reforming near practical working conditions. Journal of Membrane Science 322 (2008) 453-459.

[37] F. Gallucci, A. Basile, Pd-Ag membrane reactor for steam reforming reactions: A comparison between different fuels. International Journal of Hydrogen Energy 33 (2008) 1671-1687.

[38] P. Yaseneva, S. Pavlova, V. Sadykov, et al, Hydrogen production by steam reforming of methanol over Cu-$CeZrYO_x$-based catalysts. Catalysis Today 138 (2008) 175-182.

[39] A. Mastalir, B. Frank, A. Szizybalski, et al, Steam reforming of methanol over Cu/ZrO_2/CeO_2 catalysts: a kinetic study. Journal of Catalysis 230 (2005) 464-475.

[40] Y. Liu, T. Hayakawa, K. Suzuki, et al, Highly active copper/ceria catalysts for steam reforming of methanol. Applied Catalysis A: General 223 (2002) 137-145.

[41] P. Kurr, I. Kasatkin, F. Girgsdies, et al, Microstructural characterization of Cu/ZnO/Al_2O_3 catalysts for methanol steam reforming – A comparative study. Applied Catalysis A: General 348 (2008) 153-164

[42] B.A. Peppley, J.C. Amphlett, L.M. Kearns, et al, Methanol-steam reforming on Cu/ZnO/Al_2O_3. Part 1: the reaction network. Applied Catalysis A: General 179 (1999) 21-29.

[43] H. Purnama, T. Ressler, R.E. Jentoft, et al, CO formation/selectivity for steam reforming of methanol with a commercial CuO/ZnO/Al_2O_3 catalyst. Applied Catalysis A: General 259 (2004) 83-94.

[44] G.L. Ohl, J.L. Stein, G.E. Smith, A Dynamic Model for the Design of Methanol to Hydrogen Steam Reformers for Transportation Applications, Journal of Energy Resources Technology 126 (2) (2004) 149-158.

[45] Y. Lin, K.L. Hohn, S.M. Stagg-Williams, Hydrogen generation from methanol oxidation on supported Cu and Pt catalysts: Effects of active phases and supports. Applied Catalysis A: General 327 (2007) 164-172.

[46] S. Velu, K. Suzuki, M. Okazaki, et al, Oxidative steam reforming of methanol over CuZnAl(Zr)-Oxide Catalysts for the selective production of hydrogen for Fuel cells: Catalyst characterization and performance evaluation. Journal of Catalysis 194 (2000) 373-384.

[47] S. Murcia-Mascarós, R.M. Navarro, L. Gómez-Sainero, et al, Oxidative methanol reforming reactions on CuZnAl catalysts derived from hydrotalcite-like precursors. Journal of Catalysis 198 (2001) 338-347.

[48] S. Velu, K. Suzuki, M. P. Kapoor, et al, Selective production of hydrogen for fuel cells via oxidative steam reforming of methanol over CuZnAl(Zr)-oxide catalysts. Applied Catalysis A: General, 213 (2001) 47-63.

[49] S. Velu, K. Suzuki, T. Osaki, Oxidative steam reforming of methanol over CuZnAl(Zr)-oxide catalysts; a new and efficient method for the production of CO-free hydrogen for fuel cells. Chemical Communications, 1999 (23) 2341-2342.

[50] M. Turco, G. Bagnasco, U. Costantino, et al, Production of hydrogen from oxidative steam reforming of methanol: I. Preparation and characterization of Cu/ZnO/Al2O3 catalysts from a hydrotalcite-like LDH precursor. Journal of Catalysis, 228 (2004) 43-55.

[51] M. Turco, G. Bagnasco, U. Costantino, et al, Production of hydrogen from oxidative steam reforming of methanol: II. Catalytic activity and reaction mechanism on $Cu/ZnO/Al_2O_3$ hydrotalcite-derived catalysts. Journal of Catalysis, 228 (2004) 56-65.

[52] T. L. Reitz, P. L. Lee, K. F. Czaplewski, et al, Time-resolved XANES investigation of CuO/ZnO in the oxidative methanol reforming reaction. Journal of Catalysis, 199 (2001) 193-201.

[53] S. Sakong, A. Groß, Density functional theory study of the partial oxidation of methanol on copper surfaces. Journal of Catalysis, 231 (2005) 420-429.

[54] S. Rabe, F. Vogel, A thermogravimetric study of the partial oxidation of methanol for hydrogen production over a $Cu/ZnO/Al_2O_3$ catalyst. Applied Catalysis B: Environmental 84 (2008) 827-834.

[55] L. Zhou, S. Günther, R. Imbihl, Low-pressure methanol oxidation over a Cu(110) surface under stationary conditions: (II) adsorbate coverages and reactivity. Journal of Catalysis 232 (2005) 295-301.

[56] Y. Choi, H.G. Stenger, Kinetics, simulation and optimization of methanol steam reformer for fuel cell applications. Journal of Power Sources 142 (1-2) (2005) 81-91.

[57] S.D. Jones, L.M. Neal, H.E. Hagelin-Weaver, Steam reforming of methanol using Cu-ZnO catalysts supported on nanoparticle alumina. Applied Catalysis B: Environmental 84 (2008) 631-642.

[58] D. Chadwick, K. Zheng, The importance of water in the mechanism of methanol decomposition on ZnO. Catalysis Letters 20 (1993) 231-242.

[59] H. Yasuhisa, S. Ken-Ichiro, K. Katsuki, et al, Selective oxidation of CO in H2 by permeation through catalytically active zeolite membranes. Journal of chemical engineering of Japan 35 (2002) 1244-1251.

[60] Z. Li, W. Mi, J. Gong, et al, CO removal by two-stage methanation for polymer electrolyte fuel cell. Journal of Natural Gas Chemistry 17 (2008) 359-364.

[61] S.H. Oh, R.M. Sinkevitch, Carbon Monoxide Removal from Hydrogen-Rich Fuel Cell Feedstreams by Selective Catalytic Oxidation, Journal of Catalysis, 142 (1) 1993 254-262

[62] A. Qi, B. Peppley, K. Karan, Integrated fuel processors for fuel cell application: A review, Fuel Processing Technology. 88 (1) (2007) 3-22.

[63] P. Agnolucci, Economics and market prospects of portable fuel cells, International Journal of Hydrogen Energy 32 (17) (2007) 4319-4328.

[64] D.J. Moon, K. Sreekumar, S. D. Lee, et al., Studies on gasoline fuel processor system for fuel-cell powered vehicles applicationApplied Catalysis A: General 215 (2001) 1-9.

[65] A.S. Patil, T.G. Dubois, N. Sifer, et al., Portable fuel cell systems for America's army: technology transition to the field, Journal of Power Sources, 136 (2) (2004) 220-225.

[66] K. Yamamoto, Y. Kawamura, N. Ogura, et al., in: Proceedings of the 2004 Fuel Cell Seminar, San Antonio, TX, USA, 2004.

[67] G. Park, S. Yima, Y. Yoon, et al., Hydrogen production with integrated microchannel fuel processor using methanol for portable fuel cell systems, Journal of Power Sources, 145 (2) (2005) 702-706.

[68] A. Kundu, J.H. Jang, H.R. Lee, et al., MEMS-based micro-fuel processor for application in a cell phone, Journal of Power Sources, 162 (1) (2006) 572-578.

[69] O.J. Kwon, S.-M. Hwang, I.K. Song, et al., A silicon-based miniaturized reformer for high power electric devices, Chemical Engineering Journal 133 (1-3) (2007) 157-163.

[70] P. Rense, A. Renken, K. Hass-Santo, et al., Hydrogen production for fuel cell application in an autothermal micro-channel reactor, Chemical Engineering Journal 101 (1-3) (2004) 133-141.

[71] N. Edwards, J.C. Frost, A. Jones, et al., Self-sustaining hydrogen generator, (1998) US5,762,658.

[72] J.M. Sohn, Y.C. Byun, J.Y. Cho, et al., Development of the integrated methanol fuel processor using micro-channel patterned devices and its performance for steam reforming of methanol. International Journal of Hydrogen Energy 32 (18) (2007) 5103 - 5108.

[73] J.D. Holladay, E.O. Jones, M. Phelps, et al., Microfuel processor for use in a miniature power supply, Journal of Power Sources, 108 (1-2) (2002) 21-27.

[74] K. Shah, R. S. Besser, Understanding thermal integration issues and heat loss pathways in a planar microscale fuel processor: Demonstration of an integrated silicon microreactor-based methanol steam reformer, Chemical Engineering Journal 135 (2008) S46-S56.

[75] T. Kim, S. Kwon, Catalyst preparation for fabrication of a MEMS fuel reformer, Chemical Engineering Journal 123 (3) (2006) 93-102.

[76] A. Kundu, J. H. Jang, H. R. Lee, et al., Micro-fuel cells - Current development and applications, Journal of Power Sources 170 (1) (2007) 67-78.

[77] S. Hwang, O. J. Kwon, J. J. Kim. Method of catalyst coating in micro-reactors for methanol steam reforming, Applied Catalysis A: General 316 (1) (2007) 83-89.

[78] L. Pan, S. Wang. A compact integrated fuel-processing system for proton exchange membrane fuel cells, International Journal of Hydrogen Energy 31 (4) (2006) 447-454.

[79] D.-E. Park, T. Kim, S. Kwon, et al., Micromachined methanol steam reforming system as a hydrogen supplier for portable proton exchange membrane fuel cells, Sensors and Actuators A: Physical 135(1) (2007) 58-66.

[80] O. J. Kwon, D. H. Yoon, J.J. Kim. Silicon-based miniaturized reformer with methanol catalytic burner, Chemical Engineering Journal 140 (1-3) (2008) 466-472.

[81] D. J. Seo, W. Y, Y. Yoon, et al., Development of a micro fuel processor for PEMFCs, Electrochimica Acta, 50 (2-3) (2004) 719-723.

[82] Y. Men, G. Kolb, R. Zapf, et al., A complete miniaturized microstructured methanol fuel processor/fuel cell system for low power applications, International Journal of Hydrogen Energy, 33 (4) (2008) 1374-1382.

[83] T. Prescop, Fuel cells for portable computing and communications: Extended power away from the grid. UltraCell Corporation, 2007.

[84] O. Zerbinati, C. Campisi, F. Guglielmino, Control unit for fuel cells for portable applications. 16th World Hydrogen Energy Conference, 13-16 June 2006, Lyon, France.

[85] J. Agrell, H. Birgersson, M. Boutonnet, Steam reforming of methanol over a $Cu/ZnO/Al_2O_3$ catalyst: a kinetic analysis and strategies for suppression of CO formation, Journal of Power Sources 106 (1-2) (2002) 249-257.

[86] J. Bear. Dynamics of Fluids in Porous Media. 1988

[87] W. L. McCabe, J. C. Smith, P. Harriott. Unit operations of chemical engineering (6th). Published by McGraw-Hill Companies, Inc.

[88] S.E. Quiñones-Cisneros, C.K. Zéberg-Mikkelsen, E.H. Stenby, The friction theory (f-theory) for viscosity modeling, Fluid Phase Equilibria 169(2), (2000) 249-276.

[89] R.B. Bird, W.E. Stewart, E.N. Lightfoot, Transport Phenomena (2nd Ed.), Wiley (2002) 27-29.

[90] C.J. Jiang, D.L. Trimm, M.S. Wainwright, et al, Kinetic study of steam reforming of methanol over copper-based catalysts. Applied Catalysis A: 93 (1993) 245-255.

[91] C.J. Jiang, D.L. Trimm, M.S. Wainwright, et al, Kinetic mechanism for the reaction between methanol and water over a $Cu\text{-}ZnO\text{-}Al_2O_3$ catalyst. Applied Catalysis A: 97 (1993) 145-158.

[92] C. Chuang, Y. Chen, J.D. Ward, et al, Optimal design of an experimental methanol fuel reformer. International Journal of Hydrogen Energy 33 (2008) 7062-7073.

[93] F.P. Incropera, D.P. DeWitt, Fundamentals of Heat and Mass Transfer (5^{th} edition), J.Willey and Sons, New York, 2002

[94] C.J. Lasance, R.E. Simons, Advances In High-Performance Cooling For Electronic. 11 (2005) Number 4.

[95] H. Wang, R.B. Dinwiddie, K.E. Wilkes, et al, G-Plus report to Owens Corning- Thermal Conductivity Measurements of Fiberglass, ORNL-TM-2003/98. (April, 2003)

[96] S.V. Stankus, I.V. Savchenko, A.V. Baginskii, et al, Thermal Conductivity and Thermal Diffusivity Coefficients of 12Kh18N10T Stainless Steel in a Wide Temperature Range. High Temperature, 46 (2008) 731-733

BIOGRAPHICAL SKETCH

Jing Su was born in Tianjin, China, on January 9, 1978. He received both Bachelor of Engineering and Master of Science degrees in Chemical Engineering Department at University of Tsinghua University, Beijing, China in 2000 and 2002, respectively. Then he worked in Sunny Chemical Co. Ltd. in Shanghai and Guangdong Province of China. He entered the doctoral research program in Chemical Engineering Department at University of Florida in August 2004.